AD-A179 764 QUATERNARY NARROW-BAND SEMICONDUCTORS (HGTE)X(INSB)1-X 1/1
FOR FAR-INFRARED DETECTORS(U) SAN DIEGO STATE UNIV
FOUNDATION CA L I BERGER 31 AUG 86 N00014-83-K-0508
UNCLASSIFIED F/G 9/1 NL

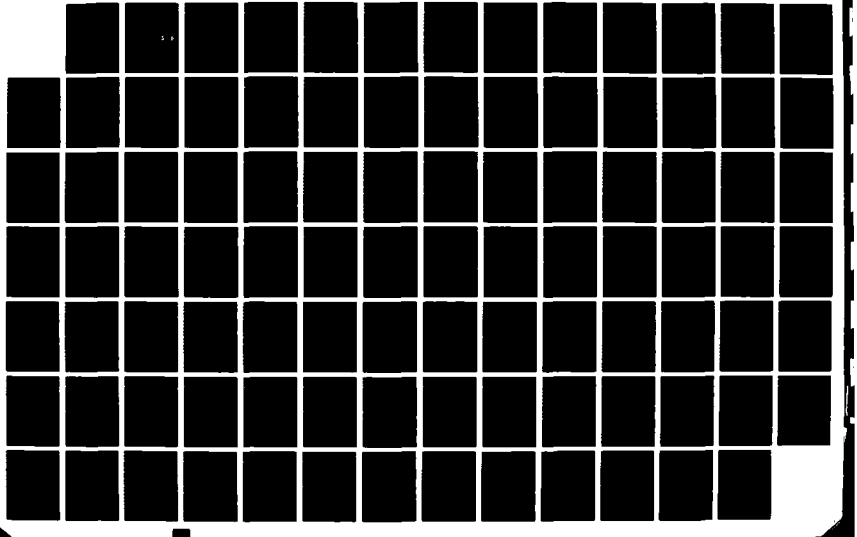

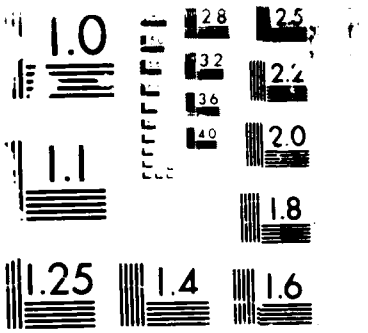
1.0
1.1
1.25
1.4
1.6
1.8
2.0
2.2
2.5
2.8
3.2
3.6
4.0

SDSU

Quaternary Narrow-band Semiconductors $(HgTe)_x (InSb)_{1-x}$ for Far-infrared Detectors

Final Report

Submitted to
Office of Naval Research
by
San Diego State University Foundation

FINAL REPORT

PROJECT TITLE: QUATERNARY NARROW-BAND SEMICONDUCTORS $(HgTe)_x(InSb)_{1-x}$ FOR FAR-INFRARED DETECTORS

GRANT NO: N00014-83-K-0588

PRINCIPAL INVESTIGATOR: LEV I. BERGER
DEPARTMENT OF PHYSICS
San Diego State University
(619) 265-6163/6240

SUBMITTED TO: OFFICE OF NAVAL RESEARCH
ARLINGTON, VIRGINIA 22217

STARTING DATE: SEPTEMBER 1, 1985

COMPLETION DATE: AUGUST 31, 1986

Lev I. Berger

LEV I. BERGER
PRINCIPAL INVESTIGATOR

CONTENTS

1. ABSTRACT

This report includes a description of results from work on an investigation of the quarternary system $(HgTe)_x(InSb)_{1-x}$ in accordance with Project N00014-83-K-0588 during the third and concluding year from September 1, 1985 to August 31, 1986.

The program of the reported year of work was, first of all, directed toward improvement of the crystal growth process with the purpose of preparation of the crystals suitable for use in the models of infrared detectors on the basis of the $(HgTe)_x(InSb)_{1-x}$ alloys (IMAT alloys). The second and main part of the program was manufacturing of the models of the IR detectors and their characterization.

It was shown that the curvature of the crystallization front in the Bridgman process could be controlled two ways, namely, by (i) a proper choice of the ratio of total length of the growing crystal to its diameter, and (ii) a controllable proportion between the radiative thermal flux and the thermal conductance flux along the axis of the ingot.

The second part of the program included preparation of the models of infrared detectors and experimental investigation of their parameters. The work was concentrated upon investigation of photoconductive detectors because of lack of information regarding the doping properties of various elements in the IMAT crystals.

The data on responsivity, noise, and detectivity combined with the data on physico-chemical and technological parameters of the crystals indicate that this group of quaternary semiconductors may be adopted in the future as effective material for low-resistance intrinsic infrared detectors and arrays for the wavelength up to the millimeter range. The undertaken research in the field of IMAT far infrared (FIR) detectors is only a first step in their investigation. The achieved level of detectivity of the IMAT detectors is about one percent of the magnitude for the MCT FIR detectors. This may be considered as a promising result taking into consideration the time periods of their investigation. Moreover, our results showed that the long-term stability of the IMAT alloys is better than that for the MCT. The advantageous physico-chemical and semiconductor properties of the group of IMAT crystals investigated (low mercury contents, lower crystallization temperature, etc.) give us reasons to conclude that any deceleration of the research in the field of these narrow-gap materials would be a disadvantage for the current attempts toward rapid progress in the field of infrared detection for both civilian and defense applications.

2. PHYSICO-CHEMICAL ANALYSIS

Our final year program included a detailed DTA of the single-crystalline (where possible) samples of the alloys after their thorough homogenization. The need for this work was dictated by the small magnitude of the mixing energy for the IMAT alloys, as it takes place in the majority of alloy systems with predominant covalent interatomic interaction [21]. This means that (a) some specifics of the material, e.g. concentration and the chemical nature of impurities, (b) incorrectly chosen temperature change rate, (c) overexposure of the alloy to high temperature followed by decomposition of the binary constituents of the alloy and formation of undesirable high temperature phases, may shift the DTA effects from their near-equilibrium magnitudes.

In this set of measurements we used Barrall's methodics [16, 22] with tin as a reference material. The choice of tin was conditioned by lack of phase transitions in it in the liquid state, the closeness of its specific heat to those of IMAT alloys, and its comparative chemical inertness to silica.

A definite amount of tin was immersed in a standard DTA ampule; the ampule was evacuated and sealed. To diminish the error from the effects connected to the difference in heat capacity between the tin and the IMAT loads, the used mass of the alloy m_x was calculated on the basis of the law of Joule and Kopp. The

mass, m_x, of an alloy of composition $(HgTe)_x(InSb)_{1-x}$ was calculated on the basis of expression

$$m_x/m_{Sn} = 0.997 + 0.386x \qquad (2.1)$$

where m_{Sn} is the mass of tin in the sealed ampule. Special attention was also paid to the similarity of geometry and mass of the used silica ampules.

The results of DTA are presented in Figure 1 together with the results of measurements on the polycrystalline samples. It can be seen that the field of solid solutions on the basis of InSb is somewhat wider, and that position of the eutectic point is shifted to the greater HgTe content (about x = 0.6).

The microhardness measurements and X-ray analysis of the single crystal samples used for DTA gave data similar to the magnitudes presented in Tables 5 and 6 of our 1985 annual report [16].

A thermodynamic analysis of chemical reactions in the systems HgTe-Sb and HgTe-In [83] showed that both In and Sb atoms react with HgTe in accordance with reaction

$$HgTe + Me \rightleftarrows MeTe + Hg \qquad (2.2)$$

as well as in the case of HgTe-Cd system. We believe that the release of mercury may be considered as a result of dissolution of Me(In) in the crystal lattice of HgTe for the case when the amount

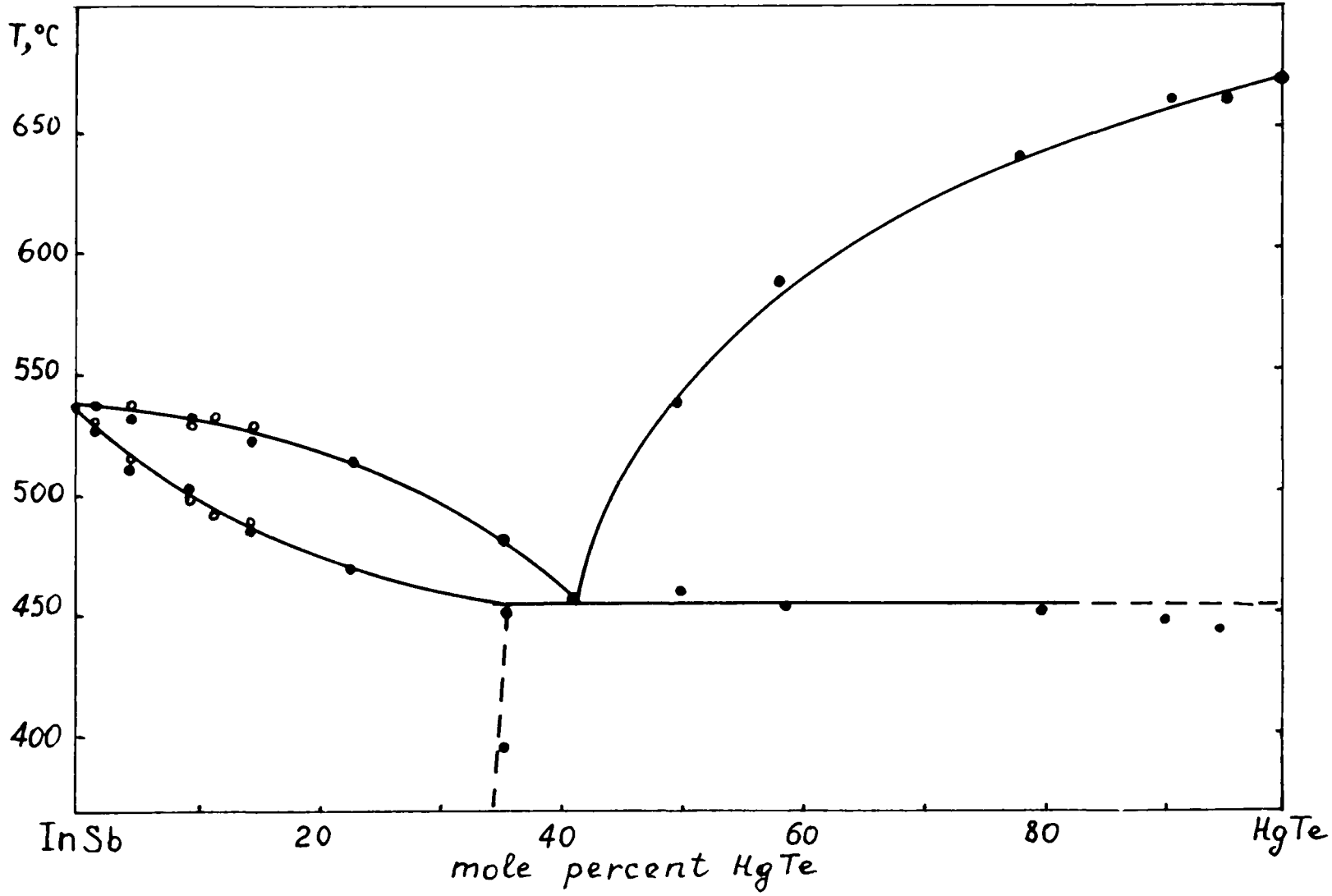

Figure 1. Phase diagram of the $(HgTe)_x(InSb)_{1-x}$ pseudobinary system, and solid line for polycrystals; o and dashed line for the single-crystalline samples.

of atoms in the anion sublattice is smaller than in the metal sublattice. If Sb is combined with HgTe, we have a similar situation because Sb atoms behave as a metal in the presence of Te. If we combine HgTe with In and Sb simultaneously, Sb atoms behave as an anion and a solid solution is created in which Hg and In occupy the cation sublattice while Sb and Te atoms form the anion sublattice. Displacement of the Hg atoms from the system will create vacancies in the lattice and consequently will not take place spontaneously (at least, up to about 800°C [83]).

3. GROWTH OF THE IMAT CRYSTALS

During the reported period, the work on improvement of the Bridgman process for crystal growth was continued. The primary aim was preparation of the detectors with the higher voltage responsivity, R_v, and detectivity, D*, and smaller generation-recombination noise, V_{gr}. In acordance with Kinch et al. [1], Borello et al. [2] and Gopal et al. [3], for low frequency and n-type single-element detector

$$R_v = \frac{\eta V_{bi} \tau n^{-1}}{lwtE_g} , \tag{3.1}$$

$$D^* = \frac{\eta}{2E_g} \left[\frac{\tau}{t} (n^{-1} + p^{-1})\right]^{1/2}, \tag{3.2}$$

and

$$V_{gr} = 2V_{bi} \left[\frac{\tau \Delta f}{lwt} \cdot \frac{1}{n(n/p+1)}\right]^{1/2}, \tag{3.3}$$

where V_{gr} is the detector bias voltage, τ is the photoconductive lifetime, l, w, and t are length, width and thickness of the element, respectively, η is the quantum efficiency of the detector, n and p represent the carrier density, and E_g is the energy gap of the detector sensor material.

From Eqn. (3.2) and in accordance with the results of our experiments, the detectors with the highest D* were made from the crystals with the lowest n. It was found that in a majority of the crystal growth runs there was a definite correlation between the curvature of the crystallization front, R^{-1}, and n: decrease of R^{-1} was followed by the n decrease.

It is possible to relate the excessive amount of the free carriers to the effects somewhat similar to constitutional supercooling in the alloy in the radial direction. These effects are determined by the ratio between the radial and axial heat flow in the melt and crystal near the crystallization front. The shape of the front can be controlled in principal by increasing the axial heat flow with respect to the radial one.

Our experiments in determination of the R^{-1} on the growing crystals consisted of dropping the ampule with the growing crystal from the furnace into water or ethylene glycol, cutting the crystal parallel to the axial plane, and investigating the border between the single crystalline and polycrystalline parts of the ingot.

The first set of experiments was devoted to investigation of the relation between the ratio L/D (L and D are the length and diameter of the ingot respectively) and R^{-1}. The average magnitude of the curvature was calculated using the expression

$$R^{-1} = 2[D^2 + (Dx-x^2-h^2)^2/h^2]^{1/2} \qquad (3.4)$$

where h is the height of the segment of crystallization front (Figure 2) and x is the depth of the crystal cut.

The parameters of the growth process were: temperature of the hot zone 800K, cold zone 723K, lowering speed 4mm/hr. The experiments showed (see Table 1) that the L/D increase relates to the decrease of R^{-1}. The magnitude of R^{-1} depends on the location of the crystallization front at the moment of quenching being somewhat greater near the middle cross section. At a given D, the magnitude of R was proportional to the length of the ingot. It was shown also that the curvature of the crystallization front changed synbatically with the charge carriers concentration. The accuracy of our experiments was high enough to measure an average curvature, but did not permit us to analyze the interface morphology as it was done in the excellent work [84]. Nevertheless, our measurements may be considered as a starting stage in the investigation of the new group of alloys. The limiting factor in our measurements was accuracy of evaluation of the magnitude of h for Eqn. (3.4). This magnitude was determined with a Leitz Microhardness Meter, Wetzlar, Germany, with Reichest Microscope Model 328061.

The second group of experiments included investigation of correlation between the shape of the Bridgman growth ampule, and the crystallization front shape, and the parameters of the growth crystals. The geometry of the used ampule is presented in Figure 3. One of them (A) is a conventional Bridgman ampule; this kind

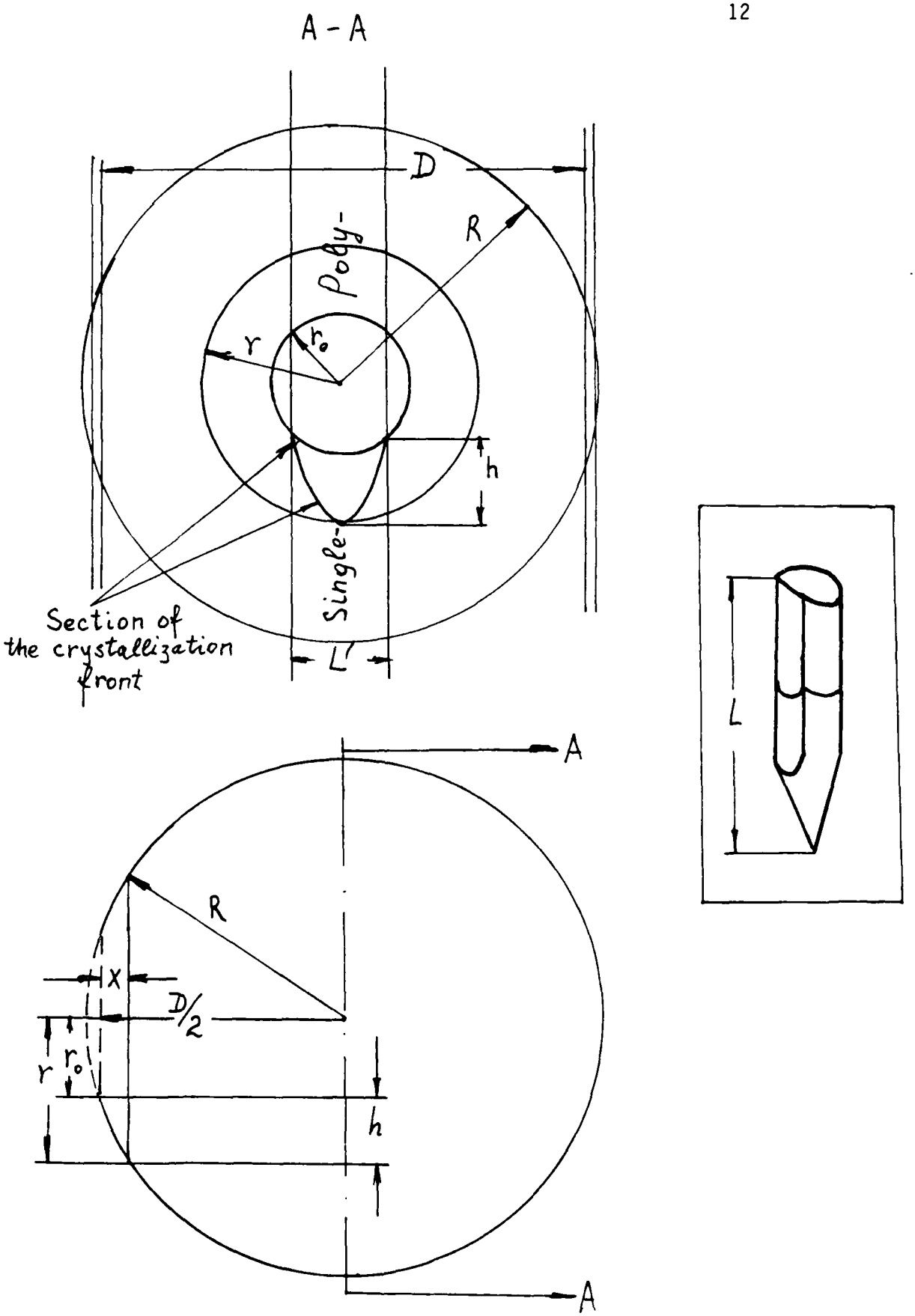

Figure 2. Geometry of the crystallization font.

TABLE 1. RESULTS OF THE BRIDGMAN GROWTH EXPERIMENTS

HgTe Contents, %	D, mm	L*, mm	R_H^{-1} m^{-1}	N_D-N_A (77K) cm^{-3}	μ_H (77K) $m^2/V \cdot s$
5	12	51	17	6.3E16	8.3
5	12	80	12	5.8E16	15.1
5	12	111	9	5.4E16	15.7
10	12	55	21	9.4E16	9.2
10	12	78	14	8.9E16	11.9
10	12	105	10	7.9E16	11.8

*The L was measured along the cylinder part of the ampule.

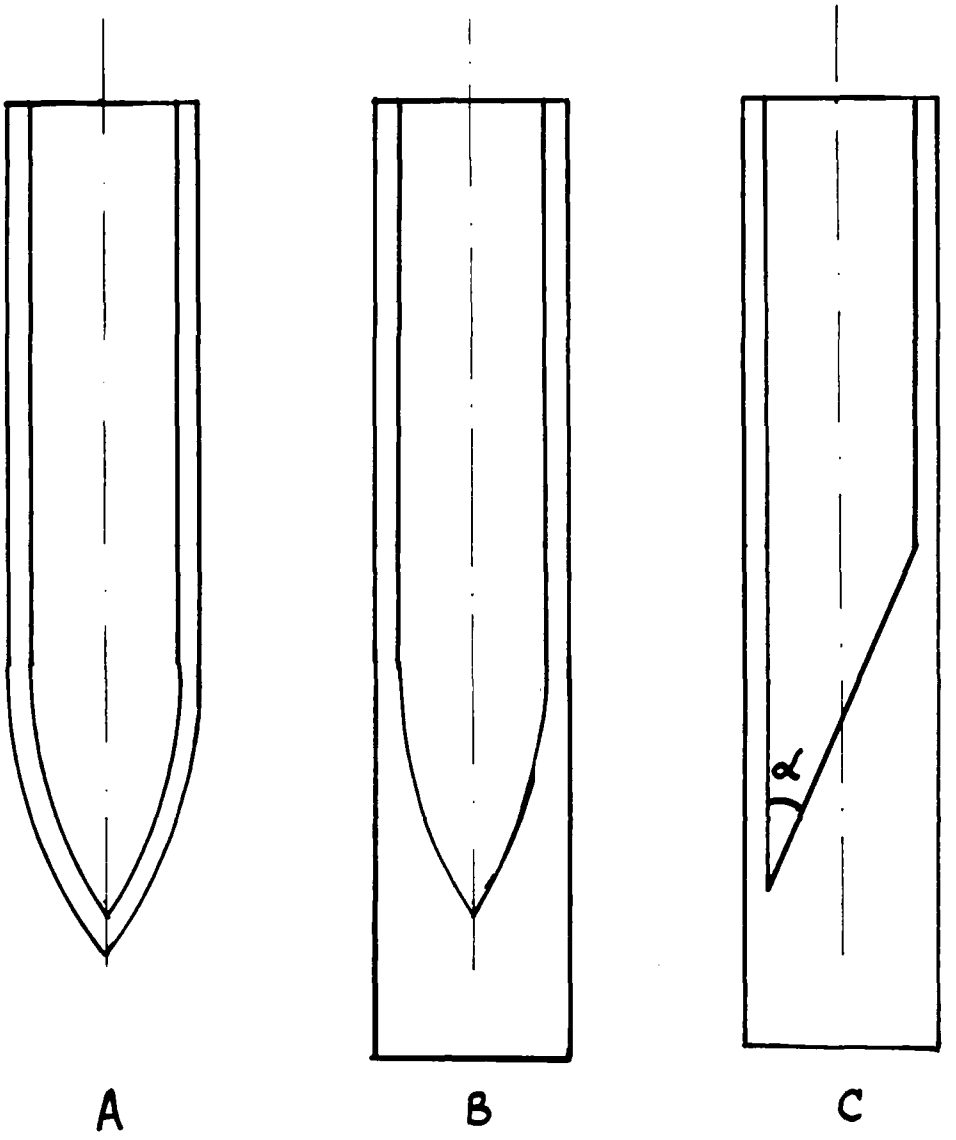

Figure 3. The ampule geometry.

of ampule was used mainly for investigation of the thermal kinematic parameters of the process, namely, temperatures in the upper and lower furnaces and their axial and radial gradients, the rate of the crystallization front motion, the curvature of the crystallization front, and their influence on the basic parameters of the grown crystals. The ampule of the shape B was designed and made in order to investigate the role of the axial gradient of temperature on the curvature of the crystallization front and the grown crystal parameters. The shape C ampule was designed to investigate a two-dimensional "blade-shaped" part of the ampule where the initial crystallization takes place. We supposed (and it was shown experimentally) that this shape might change the crystallographic orientation of the growing crystal in comparison with the one we had in a conventional ampule (Table 2). The crystals which were grown in the conventional ampule usually had [111] orientation along the ampule axis while the orientation in a shape ampule was from [100] to [110] depending on the ampule geometry, temperature and its gradient. On the basis of the results of our experiments, it can be concluded that the use of "non-traditional" ampules opens a new way to make the Bridgman-Stockbarger process more controllable and to increase the yield of good quality crystals.

The third part of our crystal growth experiments was a combination of the Bridgman technique and the vertical-zone recrystallization [4-6]. The method had been successfully used earlier for growth of the mercury-cadmium telluride crystals, and we believed

TABLE 2. ORIENTATION OF THE GROWING CRYSTALS IN THE AMPULES OF SHAPE C

X	α, rad	Temperature, K		Angle between the ampule axis and [111], rad
		Hot zone	Cold zone	
0.10	0.59	800	723	0.26
0.10	0.78	800	723	0.40
0.10	1.1	800	723	0.61

it could be effective for our alloy system. The method consists of the following operations. Stoichiometric amounts of HgTe and InSb are placed into the quartz ampule, a quartz rod with a diameter only slightly smaller than the ampule inner diameter is placed into the ampule as a stopper to such a depth that only a small space remained between the stopper and the load. After this, the ampule is connected to the vacuum system, evacuated, and sealed. The next operation consists of melting the load in the furnace where the ampule was placed vertically with its sharp end upward. The temperature in the furnace is raised slowly to the magnitude of slightly (20°C) higher than the liquidus temperature of the chosen composition. The temperature increase rate is proportional to the solubility rate of HgTe in molten InSb. After the completion of the solution process, the ampule is cooled with the furnace, then taken out from the furnace, and placed with its sharp end down into a three-temperature vertical tabular furnace (Figure 4). The temperature in the upper and lower parts of the furnace is 100°C lower than the solidus temperature and it is 25°C higher than the liquidus point of the alloy in the central part.

Initially, the ampule is in the upper part of the furnace and it is free of the alloy in its lower (sharp) end. When the ampule is lowered into the hot zone, the alloy starts to melt and the droplets of the melt flow down to the sharp ampule bottom. The speed of lowering of the ampule, the free volume of the ampule, and the length of the central zone of the furnace are chosen in such a

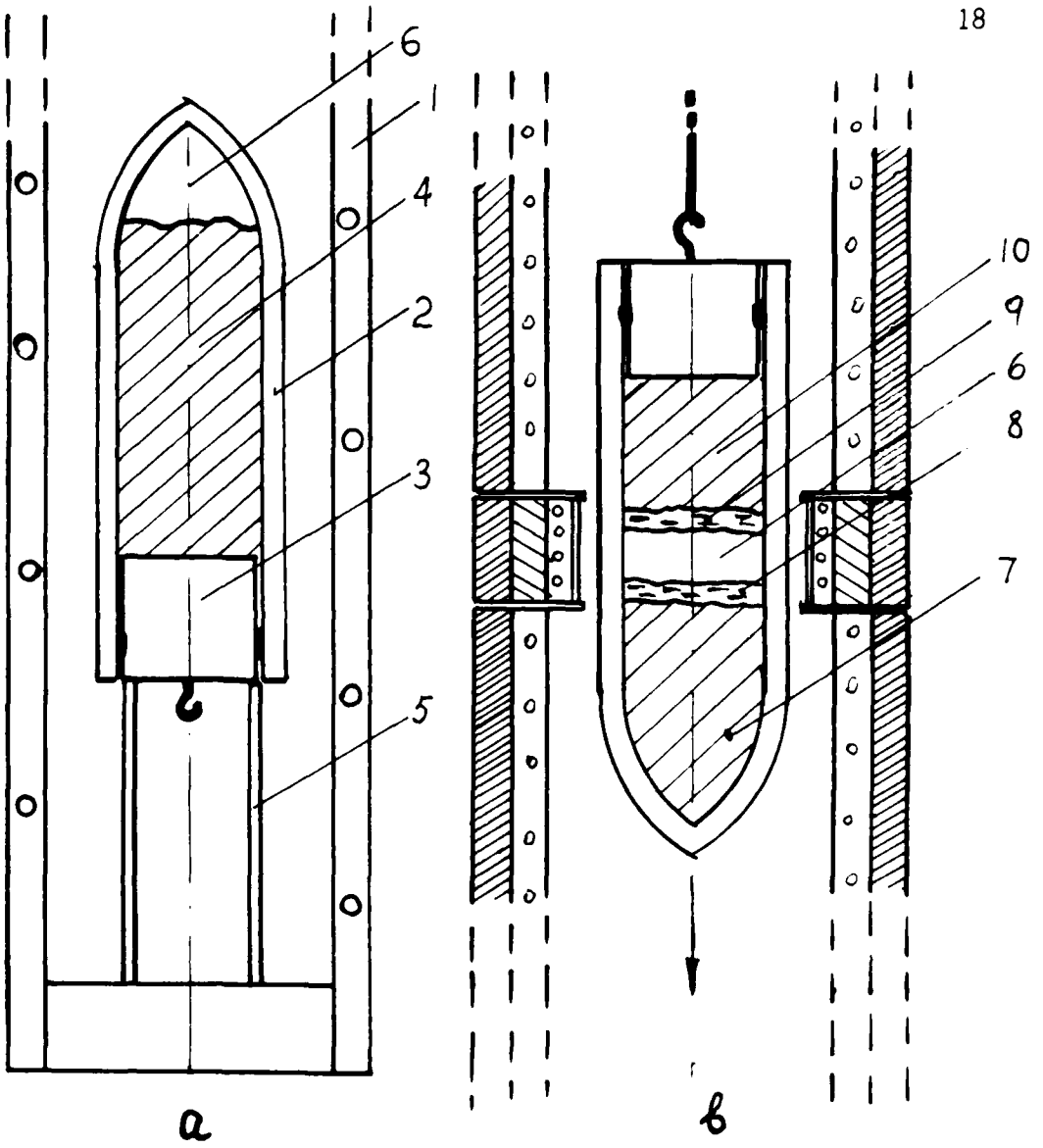

Figure 4. Combined growth technique. a--preparation of the polycrystalline alloys; b--single crystal growth; 1--furnace, 2--ampule, 3--stopper, 4--polycrystalline alloy, 5--tubular pedestal, 6--empty space, filled with gaseous components, 7--single crystalline part, 8--layer of crystalline melt on its surface, 9--layer of melt on the polycrystal, 10.

way that (a) there is a small amount of molten alloy on the top of the single-crystalline part and (b) the free space in the ampule is shorter than the length of the part of the hot zone where the temperature is equal or higher than the liquidus point. The experiments showed that single crystals were growing only in the lower part of the ampules with uniformity of the composition in the limits of one mole per cent. The composition was determined indirectly from the density measurements. Substantial difference in density of HgTe (8.170 g/cm^3) and InSb (5.775 g/cm^3) and very small change of lattice parameter with composition, following to the Vegard law, provided the accuracy of the composition evaluation within one mole per cent.

Our experiments with this method of crystal growth have to be considered as an initial stage of evaluation of its efficiency for the IMAT alloys and need a more scrupulous continuation.

4. ELECTRICAL MEASUREMENTS

Measurements of the electrical conductivity, σ, and the Hall constant, R_H, took place at 77K and 300K on the devices described before [16] in magnetic field 1T. The results of the measurements are presented in Table 3 for the crystals that were chosen for detector fabrication.

Because both InSb and HgTe are materials with very high carrier mobility, it is important, from our point of view, to discuss briefly the problem of non-ohmic behavior of the conductivity. From [85, p. 171], considering dominant interaction of current carriers with the phonons of the longitudinal acoustic mode, an expression for drift velocity of the warm electrons is

$$V_d = \mu E - 0.147 \frac{\mu_o^3}{u_1^2} E^3 \qquad (4.1)$$

and for the hot electrons

$$V_d = 1.81 (u_1 \cdot \mu_o)^{1/2} E^{1/2} \qquad (4.2)$$

where μ_o is mobility at $E \approx 0$, u_1 is the longitudinal wave speed, and E is the intensity of the applied electric field. The magnitude of E at which deviations from Ohm's law become significant is (at $\frac{\mu-\mu_o}{\mu_o} = 10\%$) from (4.1):

TABLE 3. ELECTRICAL PARAMETERS OF THE (HgTe) (InSb) CRYSTALS USED FOR INFRARED DETECTOR FABRICATION

Sample No.	X	σ, $(\Omega cm)^{-1}$		n, $10^{16} cm^{-3}$		μ_H, $m^2/V \cdot s$	
		77K	300K	77K	300K	77K	300K
51014	0.12	917	1380	2.1	5.5	27.3	15.7
51028	0.12	913	1150	3.3	7.0	17.3	10.3
51111	0.10	1300	1320	5.4	7.3	15.1	11.3
51126	0.12	1030	1450	4.1	6.9	15.7	13.1
51208	0.10	1490	1300	7.9	8.9	11.8	9.1
60113	0.12	947	810	3.4	6.1	17.4	8.3
60217	0.12	945	1470	2.8	5.3	21.1	17.3
60421	0.10	1380	1410	9.4	9.9	9.2	8.9
60518	0.10	1840	1660	13.1	14.2	8.8	7.3
60601	0.10	1110	1700	4.2	7.2	16.5	14.8

$$E_c = 0.8 \frac{u_1}{\mu_o} \approx \frac{u_1}{\mu_o} \tag{7}$$

Let us estimate the magnitude of E_c for HgTe and InSb on the basis of the known data. A simplified assumption

$$u_1 = (C_{11}/D)^{1/2} \tag{8}$$

where C_{11} is one of the elastic constants of the crystal and D is its density is used for calculation. The results of calculations are presented in Table 4. It is seen that the IMAT material has E_c substantially greater than for pure InSb. This result agrees well with both theoretical [90] and experimental [91] results of investigation of mobility of solid solutions. It is worthwhile to mention that E_c of the IMAT and MCT crystals is of the same order of magnitude; this means that the voltage photoresponse for the IMAT is not limited by the bias voltage in comparison with the MCT.

TABLE 4. CALCULATION OF THE CRITICAL FIELD STRENGTH

Material	Density g/cm^3	C_{11} $10^{11} dn/cm^2$	u_l km/s	$\mu_{on}(77K)$ $m^2/V \cdot s$	E_c V/cm
InSb	5.78	6.7 [86,87]	3.4	51 [16]	0.7
HgTe	8.17	5.4 [88,89]	2.6	7 [67]	3.7
$(HgTe)_{0.1}(InSb)_{0.9}$	6.02	7.0 (est.)	3.4	12 (ave.)	2.8

5. DETECTOR FABRICATION

Detectors were fabricated mainly on the silicon single crystal substrates. A piece of $(HgTe)_x(InSb)_{1-x}$ was mounted on the substrate with epoxy resin and mechanically and chemically polished to the thickness of about 20-40 μm. The initial dimensions of the piece were about 10 x 1 x 1 mm^3, and, after lapping and indium electrodes deposition, the dimensions of the working part of the detector were about 1 x 1 x 0.03 mm^3. The copper bonding wires were soldered to the indium electrodes.

Before epoxying the slab to the substrate, the surface of it faced to the substrate was very thoroughly lapped with alumina powder and etched in the mixture of HF: HNO_3:CH_3COOH = 1:1:1.* This was done because of the importance of the low surface recombination not only on the front surface of a PC detector but also on its back surface.

For epoxying, the "five-minute" epoxy glue of Lactite Corp. was successfully used (300K).

In our experiments, we used as substrates either high resistivity silicon wafers or microscope glass slides. None of our experiments had complications in connection with an inadvertent electrical contact between the slab and the silicon substrate.

---

*In some experiments, the mixtures HCl:HNO_3:H_2O = 1:2:3 and Br:CH_3OH = 1:4 were used.

Our preference to silicon is conditioned by the closeness of the thermal expansion coefficients of silicon ($4.2 \times 10^{-6}\ K^{-1}$), HgTe ($5 \times 10^{-6}\ K^{-1}$ [10, 11]), and InSb ($4.67 \times 10^{-6}\ K^{-1}$ [12]), whereas the average magnitude of the coefficient for the microscope slide glass is about $8 \times 10^{-6}\ K^{-1}$.

The electric contacts were made by soldering the copper wire (diameter 10 μm) to the outer surface of the slab which was polished and etched to the thickness of about 20-40 μm. In some experiments, silver paste was used for the wire bonding. The contact rectification test showed some evidence of non-ohmic behavior but only in the limits of a small percent.

Because our experiments were only the initial steps of investigation of the new class of infrared detection materials, we did not include in our schedule questions regarding the antireflecting coating, passivation of the working surface of the detectors, and housing design.

6. CHARACTERIZATION OF DETECTORS

Characterization of a set of detectors was based upon the results of the resistivity, Hall effect, and photoelectric lifetime measurements. The following assumptions were accepted: (i) the crystals have near intrinsic conductivity; (ii) effective masses are equal to $m_e = 0.014\ m_o$ and $m_p = 0.40\ m_o$ in InSb, and $m_e = 0.017\ m_o$ and $m_p = 0.50\ m_o$ in HgTe; (iii) the mobility ratio is equal to $b = 104$ for InSb and $b = 71.4$ for HgTe; (iv) the magnitude of b in the solid solution crystals is a linear function of composition. On the basis of these assumptions:

$$\sigma = ne\mu_n(1 + b^{-1}) \approx ne\mu_n \tag{6.1}$$

Combining (6.1) and (3.1) yields

$$R_v = V_{bi} \cdot \frac{\eta\tau R_D e\mu_n}{lwE_g}\ , \tag{6.2}$$

where R_D is the measured magnitude of the detector resistance, e is the electron charge. Combining (3.2) and (6.1) yields

$$D^* = \frac{\eta}{2E_g}\left(R_D\ e\mu_n\tau\right)^{1/2} \tag{6.3}$$

and from (6.2) and (6.3):

$$R_v = \frac{4E_g(D^*)^2}{\eta w n} \cdot V_{bi} \tag{6.4}$$

Equation (6.3) is similar to one offered by Kingston [13, p. 64] for the incident photon energy near to the energy gap. In this consideration, in accordance with our experiments, we assume that $l \approx w$.

Another useful expression for our analysis is

$$P_{NE} = \frac{(\Delta f A)^{1/2}}{D^*} \tag{6.5}$$

where P_{NE} is the noise-equivalent power and A is the irradiated detector area; this is a combination of the formulas for the experimental detector characterization [14, p. 4].

$$P_{NE} = \frac{P_D A}{S/N} \tag{6.6}$$

and

$$D^* = \frac{S/N}{P_D} \left(\frac{\Delta f}{A}\right)^{1/2} \tag{6.7}$$

where S/N is the ratio of signal and noise and P_D is the radiant power density at the surface of the detector.

The quantum efficiency of the detector may be determined by the expression [15]

$$\eta = \frac{(1-R)(1-e^{-\alpha t})}{1-Re^{-\alpha t}} \tag{6.8}$$

where R is the reflectivity that depends on the refractive index n_r:

$$R \approx (n_r - 1)^2 (n_r + 1)^{-2}$$

Total noise V_T is equal

$$V_T = (V_{gr}^2 + V_{th}^2)^{1/2} \tag{6.9}$$

where V_{gr} is the generation-recombination noise (see Eqn. (3.3) and V_{th} is the thermal noise

$$V_{th} = (4kTR_D\Delta f)^{1/2}, \tag{6.10}$$

k is the Boltzmann constant.

In the case of "almost intrinsic conductivity, Eqn. (3.3) may be rewritten as

$$V_{gr} = V_{bi} \left(\frac{2\tau\Delta f}{nlwt}\right)^{1/2} \tag{6.11}$$

For T = 77k, Eqn. (6.10) may be presented in the form

$$\frac{V_{th}}{(\Delta f)^{1/2}}, \ V/Hz^{1/2} = 6.5 \times 10^{-11} \ R_D^{1/2}, \ (Ohm)^{1/2} \tag{6.12}$$

Whereas for the generation-recombination noise

$$\frac{V_{gr}}{(\Delta f)^{1/2}} = V_{bi} \left(\frac{2\tau}{n l w t}\right)^{1/2} . \tag{6.13}$$

From our data, taking V_{bi} = 10mV, Eqn. (6.13) gives

$$\frac{V_{g\text{-}r}}{(\Delta f)^{1/2}} \approx 10^{-12}\ V \cdot Hz^{-1/2} \tag{6.14}$$

which means that in our detectors, total noise depends mainly on its Johnson component, and the expression for the spectral detectivity may be presented [7] in the form

$$D^*_\lambda = \frac{R_v}{R_D^{1/2}} \left(\frac{lw}{4kT}\right)^{1/2} \tag{6.15}$$

without a substantial loss in accuracy.

7. EXPERIMENTAL INVESTIGATION PERFORMANCE OF THE DETECTORS

In the previous section we discussed a "normalized" performance of the detectors, based mainly on the results of electrical and galvano-magnetic measurements.

Our experiments, being limited by time, were performed at one operating mode, namely, the detector temperature 77K and the CO_2 laser (λ = 10.6 μm) as the source of IR radiation.

The detector was mounted in the Dewar [16, p. 45]. The high resistivity $\sim$0.5 mm thick silicon disk was used as a long wave pass filter. In our system, the field of view was about 50°; it gave us the minimum noise equivalent power of the order of 10^{-13} W (see, e.g. [17, p. 327] for a case of the BLIP detector) which is about two orders of magnitude smaller than our experimental data.

The beam from a CO_2 laser, chopped at various frequencies to 100 Hz, was used as a measured signal. The lengths and widths of the detectors were distributed within the range of 1-2 mm. The two photoconductive detector characteristics, namely, responsivity and detectivity were measured for all detectors.

The electric measuring circuit used for our experiments is shown in Figure 5. It is similar to one used by Keyes and Quist [17, p. 341]. A limitation of "almost-intrinsic" HgTe-InSb as a low resistance (in our experiments) material is the magnitude of the electric field that can be applied to the detector without

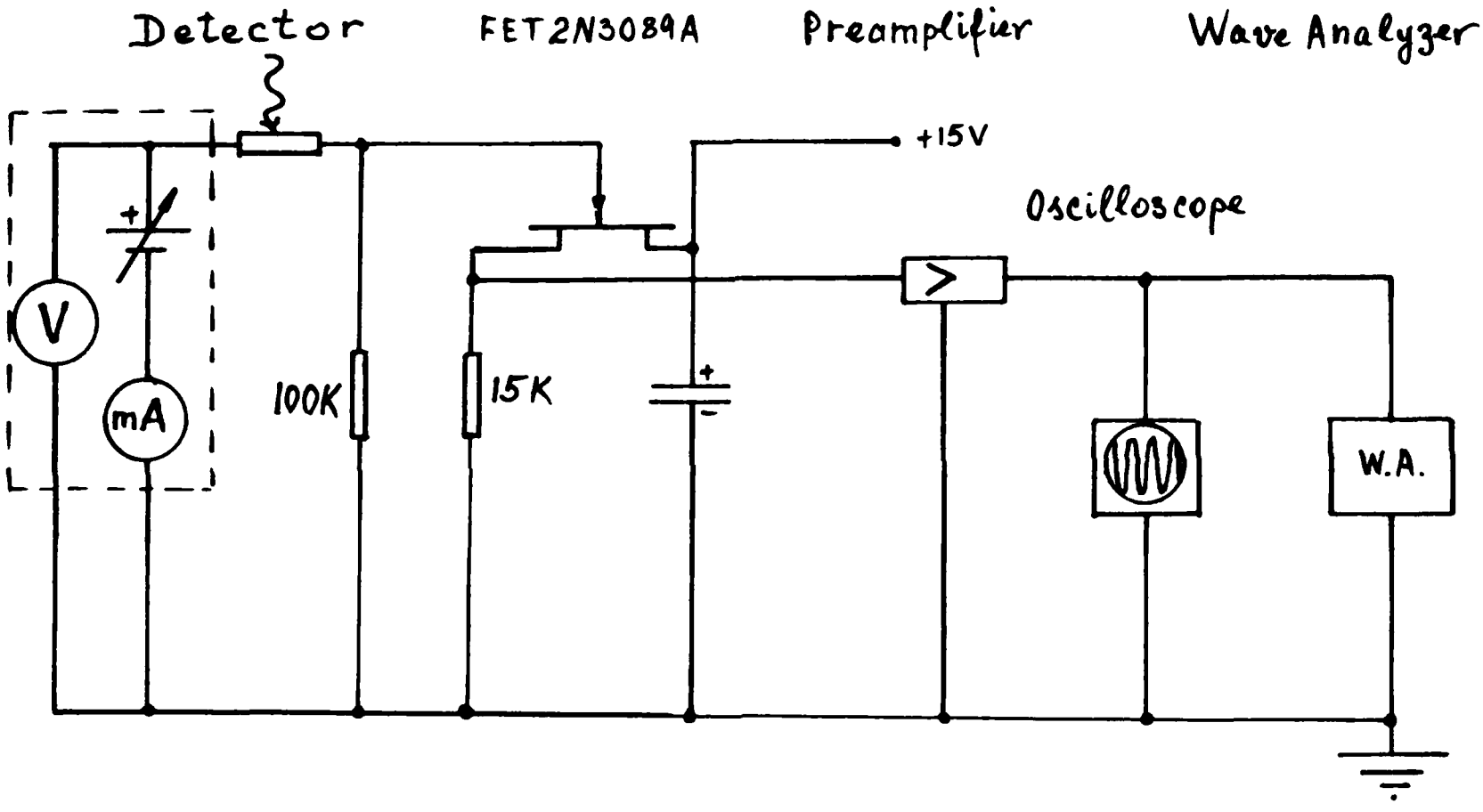

Figure 5. The electrical circuit for the responsivity and detectivity measurements.

breakdown. In our experiments, the upper limit for electric field in the detectors was 0.5 V/cm.

The results of the calculations and measurements are found in Table 5. Comparison of magnitudes of D* calculated by using Eqn. (3.2) with the results of the detector performance measurement (Eqn. 6.7) shows a satisfactory agreement. This result may be considered as proof of the Shockley-Read type recombination mechanism in the $(HgTe)_x(InSb)_{1-x}$ crystals with $\tau_n = \tau_p$ [18].

The detectors with $x < 0.1$ were sensitive to the IR radiation only at the chopping frequencies below 25 Hz and the signal-to-noise ratio was reverse proportional to the frequency. It may be considered as evidence of the bolometric response [23].

Our results were compared with the background-limited detectivity D^*_{BLIP} [9]:

$$D^*_{BLIP} = \left(\frac{\eta}{2P_B}\right)^{1/2}/h\nu = \left(\frac{\lambda^2\eta}{2P_B}\right)^{1/2}/hc \qquad (7.1)$$

where $P_B = 4.7 \times 10^{14}$ photons/(s·cm^2) is the photon flux from the background at 300K. If $\lambda = 10.6$ μm and $\eta = 1$,

$$D^*_{BLIP} = 1.7 \times 10^{12}\text{cm Hz}^{1/2}\cdot\text{W}^{-1} \qquad (7.2)$$

The experimentally achieved magnitude of D* is of the order of 0.1 per cent of the theoretical maximum that may be considered as a

TABLE 5

DETECTOR PARAMETERS

Detector		Dark resistance, Ω		D^*_{77K} (calc.)	τ_{PC}	D^*_{77K} (exp.)	P_{NE}	R_v	Noise (total)
Number	X	77K	300K	cm $Hz^{1/2}/nW$	μs 77K	cm $Hz^{1/2}/nW$	pW	V/W	$pV/Hz^{1/2}$
351014	0.12	0.37	0.24	5.59	0.83	3.08	73	1.22	40
151028	0.12	0.40	0.27	4.45	1.1	2.87	78	1.18	41
251111	0.10	0.25	0.25	3.49	0.75	1.75	128	0.57	33
351126	0.12	0.32	0.23	4.01	0.81	2.10	107	0.77	37
251208	0.10	0.22	0.25	2.88	0.67	1.37	163	0.42	31
460113	0.12	0.35	0.41	4.40	0.84	2.35	95	0.90	39
160217	0.12	0.35	0.22	4.85	0.86	2.62	85	1.01	39
460421	0.10	0.24	0.23	2.64	0.76	1.35	166	0.43	32
160518	0.10	0.18	0.21	2.24	0.61	1.02	219	0.28	28
160601	0.10	0.30	0.19	3.95	0.80	2.07	108	0.73	36

Comments: λ = 10.6 μm; i_{bias} = 40-400 μA; ν_{chop} = 90 Hz.

promising result for the material which was synthesized first only about three years ago.

8. THE LONG-TERM STABILITY OF THE IMATS

As we mentioned in our previous reports [16] for this project, there were several reports concerning changes in the electrical parameters, conduction type, and/or optical properties of MCT stored at room temperature for periods of 3-13 years [75-78]. The observed changes differ in degree with the preparation technique. They include such changes as a reduction in the free charge lifetime [78], an increase in thickness of a p-type core of the n-type bulk crystals [76], as well as other differences in electrical, optical, and/or mechanical properties [77].

A possible explanation for this disadvantage to the FIR MCT consists in the fact that these materials are somewhat dilute solid solutions of CdTe in HgTe. High rate of the Hg sublimation creates the need to have some excess of mercury over stoichiometric composition in the initial mixture prepared for synthesis. Part of this Hg exists in the initial melt of MCT in the shape of tiny droplets. These droplets are very stable (surface tension of the Hg metal at 700°C is 500 N/m [79]), and a portion of them may still exist in the material even after its crystallization. A painstaking heat treatment helps to dissolve these droplets in the crystal, but a substantial amount of the mercury atoms may still occupy interstitials, stacking faults, etc. If the Hg atoms from the surface sublimate, the mercury vacancies will migrate into the bulk of the

crystal, the atoms from the imperfections will diffuse into vacancies with their following motion to the surface, and so on.

From the results [80] of investigation of the Hg diffusion in MCT at low temperatures, we could conclude that a minimum duration of our experimental investigation of the long-term stability of the MITA alloys must be three years. At the beginning of our project, we had only the polycrystal alloys, and we had used them for this set of experiments having in mind that, if we waited for the moment when the single crystals would be available, the test time would be insufficient.

For our test, we used only one parameter: electrical resistance at room temperature by the collinear four-probe array probe [81]. The tested samples were discs with a diameter 12 mm and thickness 1-2 mm. They were cut out from the IMAT ingots with $x = 0.05$, $x = 0.10$, and $x = 0.15$. The ingots were annealed after synthesis during 100 h. The conductivity data were taken in six positions on each side of the polished, etched, thoroughly rinsed, and dried discs.

After measurements, the discs were loaded in the silica ampules, one of each composition. After loading, one ampule was closed by a cork stopper, and a second ampule was connected to the vacuum system, evacuated, and sealed. The third ampule was also evacuated and sealed, but its contents included also a certain amount of free mercury.

The ampules were kept at room temperature inside of a ventilated hood during the time period from November 23, 1983 to September 10, 1986, when the samples were taken out from the ampules and their electric conductivity was measured again at the similar conditions. The results are presented in Table 6. From these results, it can be seen that in the limits of the experiment accuracy the magnitude of electrical conductivity did not vary during the test period. From our point of view, this fact has the following explanation.

Evaporation of mercury from the surface is followed by creation of vacancies. Migration of these vacancies into the bulk of crystal will be followed by the motion in the direction of the surface by a majority of the atoms, in our case, those of indium. This will create near the crystal surface a layer of material with relatively low partial vapor pressure. The layer will decrease access of mercury atoms to the surface and so stabilize composition of the alloy crystal. The thickness of this layer (a few lattice parameters) is much smaller than the FIR wave length and its cut-off wave length is also shorter than the one of the detected radiation. Consequently, this layer being an obstacle for migration of the mercury atoms to the surface stabilizes the composition of the IMAT crystal without any substantial change of the crystal properties. As an additional argument for preferable migration of the In atoms to the surface mercury vacancies is their so-called covalent radius [74]:

TABLE 6

RESULTS OF THE ELECTRICAL MEASUREMENTS

Sample No.	X	Average electrical conductivity, $(\Omega \cdot cm)^{-1}$			
		November 1983		September 1986	
		Side 1	Side 2	Side 1	Side 2
1U	0.05	108	99	115	90
2U	0.10	230	210	207	220
3U	0.15	160	180	180	170
4V	0.05	115	120	110	120
5V	0.10	220	220	210	210
6V	0.15	165	170	160	170
7M	0.05	105	110	110	100
8M	0.10	230	230	220	250
9M	0.15	170	180	190	180

Comments:

1. Letters, U, V, and M are for the unevacuated, evacuated and sealed with mercury ampules respectively.

2. Deviation from the average on all samples was in the limits ± 15%.

Element	Hg	In	Sb	Te
Radius, Å	1.54	1.48	1.35	1.28

For comparison, the magnitude for Cd is 1.56 Å. Diffusion of an indium atom from one Hg vacancy to another through the crystal is apparently more probable than for the mercury atoms. One can see that in the case of the MCT alloys the situation is just opposite; mercury atoms possess smaller radius and contents of mercury in the FIR MCT alloys is much higher than the other metal constituent (cadmium).

A detailed investigation of the diffusion mechanism in the IMAT's is out of the frame of this project and might be a subject of a separate investigation. Some idea about diffusion of mercury and indium may be taken from comparison of the results of investigation of mercury diffusion [78] with those of indium in MCT [82].

9. DISCUSSION OF THE RESULTS

9.1 Material Preparation

The composition range of semiconductors in the system $(HgTe)_x(InSb)_{1-x}$ spans the x magnitudes from zero to ~0.3. The results of our experiments have shown that the optimal composition from the viewpoint both of device efficiency and material technology is x = 0.12 for the 8-14 μm IMAT infrared detectors.

Relatively low content of mercury in the alloy with x = 0.12 (9.70 weight per cent, cf. 51.7% in $Hg_{0.8}Cd_{0.2}Te$) provides conditions of crystal growth quite similar to those for InSb; and we know that indium antimonide is essentially the only III-V compound that can be prepared in single crystal form by conventional means. In our investigation, growth of the x = 0.12 crystals by the Bridgman technique was successful almost from the very beginning of its application.

We found that the temperature gradient near the crystallization front did not need to be greater than 25-30 K/cm. Satisfactory quality crystals may be grown at the speed up to 1.1 μm/s. Comparison of the quality of grown crystals with the temperature distribution along the direction of growth indicated that the temperatures in the "hot" and "cold" parts of the furnace must be chosen so that the temperature gradient is a constant on both sides of the crystallization front. This condition ($\partial^2T/\partial Z^2 = 0$) can be

satisfied easily if the crystallization front is located near the middle of the space that separates the hot and cold zones of the furnace.

As a rule, a greater temperature gradient in the melt near the surface of a growing crystal was followed by an increase in the nonuniformity of electrical properties. The experiments showed that the best uniformity for the crystals with X = 0.12 was achieved at the temperature gradient 22 K/cm and linear distribution of temperature in the limits 10-15 mm from both sides of the crystallization front (measured along the axis of the growing crystal).

In spite of a certain reproducibility of the results (see Table 7), we believe that our results are only the first steps in investigation of the IMAT crystals. The subsequent steps of the bulk crystals preparation have to include investigation of lattice defects and their influence on the electrical and optical properties, distribution of impurities in the crystals, and detailed investigation of the axial and radial nonuniformity of composition, its dependence on the methods of heat treatment, diffusion processes in the alloys, and correlation of the electric parameters with composition and partial pressure in the gas phase during the growth process.

In our experiments, we used two methods of thin film growth--hot-wall epitaxy and evaporation-diffusion at isothermal conditions. Essentially, both methods include diffusion of HgTe into

TABLE 7

GROWTH PARAMETERS OF $(HgTe)_{0.12}(InSb)_{0.88}$ CRYSTALS

Run No.	Temperature, K: Hot zone	Cold zone	Annealing	Growth speed, mm/hr	Single crystal length, mm	Crystal description
11-1	786	710	710	4	43	Single crystal, little spots of Hg on the surface
13-1	772	706	706	4	20	Single crystal no free Hg, shiny surface
15-2	803	710	573	4	40	Same
17-1	800	723	690	4	73	Same

the InSb substrate, and as is known, this process will create a concentration gradient normal to the plane of the growing film. It is not as critical in the IMAT layers as it is in the MCT layers because the optical properties of the former do not depend on their composition gradient as to the latter ones. Nevertheless, we may expect better uniformity of the layers and better IR detector parameters of the epitaxial layers grown from independent and controllable sources of Hg, In, Sb, and Te by methods such as MBE and especially MOVPE. Adjustment of these methods and an investigation as to their efficiency is a goal of our future work.

9.2 Electrical Properties

Our work showed that $(HgTe)_{0.12}(InSb)_{0.88}$ single crystals have a relatively high electron mobility and lifetime. These two parameters provide expectations of making the high performance infrared detectors. Another critical parameter of semiconductor material for IR detectors is the free charge concentration. As is usual, we started from polycrystals with a concentration up to $10^{19}cm^{-3}$. In the single crystals, concentration decreased to $10^{17}cm^{-3}$ and after a properly chosen heat treatment, to $10^{16}cm^{-3}$. Nevertheless, a weak dependence of concentration on temperature indicates that our material may include a substantial amount of impurity atoms and lattice defects as also took place, for example, in the first steps of investigation of InSb and MCT. As a result of the elevated free charge concentration, the detectivity of the IMAT detectors is on the level of $10^{9}cm \cdot Hz^{1/2}/W$ which is about 1 per cent of the magnitude for the MCT photoconductive detectors. But the latter have behind them almost 30 years of work toward their improvement by numerous groups of scientists and engineers, whereas the IMAT materials only attracted interest about three years ago. It is possible that by some relatively common means, such as annealing [100], the current carrier concentration may be decreased to, say, $10^{14}1/cm^{3}$ with a corresponding increase of detectivity and responsivity of the IMAT detectors.

The electrical parameters of the grown epitaxial layers are characterized by the mobility on the level 10^{2}-$10^{3}cm^{2}/V \cdot S$ and high

concentration of the current carriers. The current status of work on their preparation and investigation may be considered as but the very beginning, and it will take a certain period of time before the IR detectors on their basis will be of competitive quality. As was mentioned earlier, the work has to be aimed toward the achievement of compositional uniformity and improved defect concentration. Our plans for subsequent work include epitaxial growth of IMAT films by, first of all, the MOCVD as their most important part. In particular, we are considering concentration of our attention on investigation of the process of photolytic and radiolytic metal-organic vapor phase epitaxy (see Appendix).

For understanding the transport phenomena in the IMAT alloys, it is important to have information regarding their band structure and effective mass. There have been a limited amount of attempts to calculate the correlation between the electron (hole) energy and the wave vector. One of them was undertaken by Kane [101] for InSb with $\vec{k} \approx 0$ and introduction of a spin-orbit coupling parameter. Kane's model is very simplified (the anisotropy of the valence band is neglected, etc.), and even now the information regarding energy gaps and effective masses can be reliably obtained only from such experiments as optical absorption and reflection and cyclotron resonance. These experiments are a part of our future work with the InSb-rich IMAT crystals and films.

9.3 Optical Properties

As is common for narrow-band semiconductors, several mechanisms of the photon absorption control the light transmission. As an example, Figure 6 represents a transmission curve for the crystal $(HgTe)_{0.05}(InSb)_{0.95}$ at 77K. A kink on the curve T = T(hv) takes place near λ = 13 μm which is close to the cut-off wave length. If we use the hydrogen model of excitons, their binding energy may be estimated from the expression [102]

$$\Delta E_{exc} = - \frac{m_a e^4}{8h^2(\varepsilon\varepsilon_o)^2} \cdot \frac{1}{n^2} \qquad (n = 1, 2, 3, \ldots) \qquad (9.1)$$

where m_a is the "normalized" mass,

$$m_a^{-1} = m_n^{-1} + m_p^{-1},$$

e is the electron charge, and $\varepsilon\varepsilon_o$ is the static dielectric susceptibility. Calculations of ΔE_{exc} for pure InSb which have parameters close to $(HgTe)_{0.05}(InSb)_{0.95}$ gives the magnitude $\Delta E_{exc} \approx 10^{-1}$meV. At 77K, exciton levels below the absorption edge can only give a kink on the absorption curve as can be seen, for example, on the curve for GaAs [103]. Another factor that screens the electron-hole interaction is the large current carrier concentration (10^{16} 1/cm) that takes place in the crystals we used for optical experiments. It is worthwhile to mention that our data are similar to the results of Hrostowski et al. [104] for n-InSb in the first

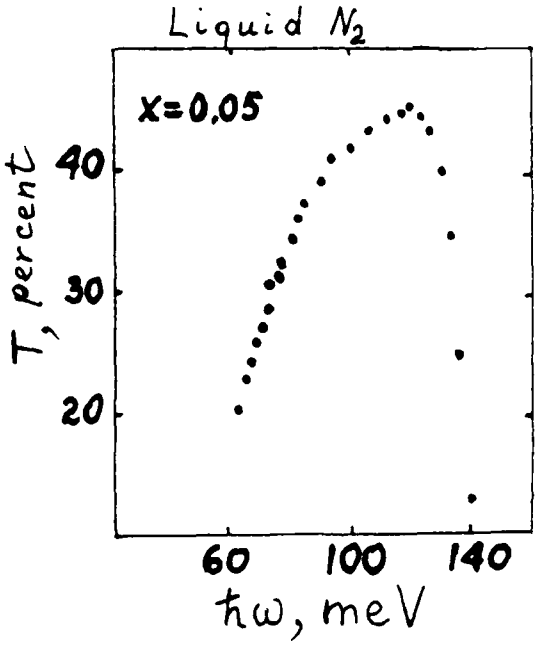

Figure 6. Transmittance of a $(HgTe)_{0.05}(InSb)_{0.85}$ single crystal.

steps of investigation of optical properties of the samples with relatively high (from $\sim 10^{16}$ to 10^{19} $1/cm^3$) free charge concentration. This work will be continued in the future on better quality crystals and films and at lower temperatures.

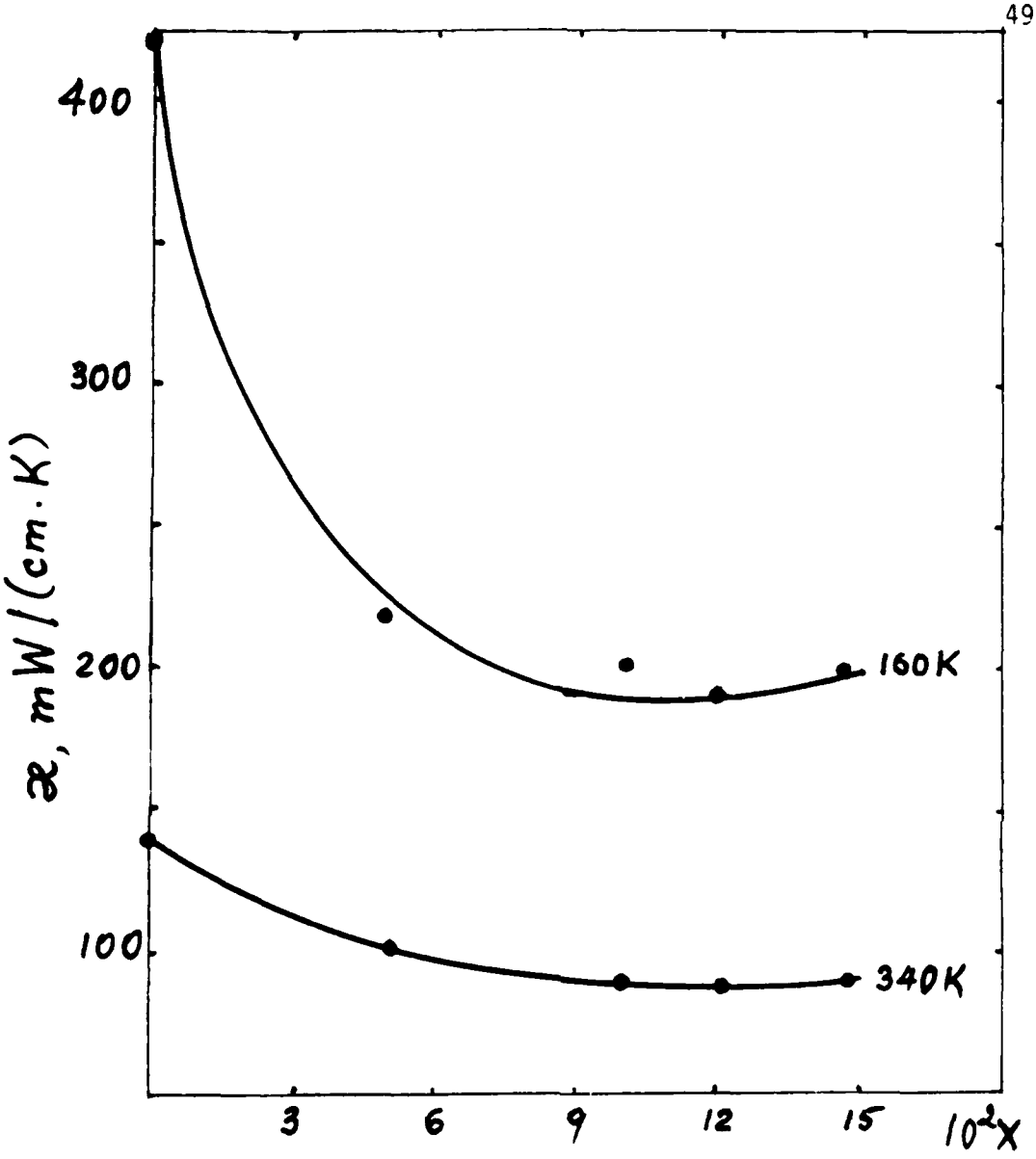

Figure 7. Dependence of the thermal conductivity of a group of the IMAT single crystals on HgTe contents.

9.4 Thermal Conductivity and Thermal Expansion

During the last year of the project, we investigated temperature dependence of thermal conductivity, κ, within the limits 160K to 340K. The purpose of these experiments was twofold: (a) evaluation of the temperature and composition dependence of κ to use these data for the future crystal growth and detector design, and (b) estimation of the electron and phonon parts of κ. Dependence of κ on composition in the chosen temperature range is presented in Figure 7. There is an important feature of the curves: the rate of change of κ with composition is greater at lower temperatures and goes through zero near $x \approx 0.11$. Another important conclusion can be formulated on the basis of the curves of Figure 8. Dependence of κ on reciprocal temperature is linear for the majority of the samples used. This means that κ is limited mainly by phonon-phonon interaction. The non-linear part of the InSb curve may be explained by an electron contribution to the total thermal conductivity. It makes sense to mention that the alloy single crystals (a) have κ substantially smaller than κ of InSb and (b) their κ is changing with x relatively slowly.

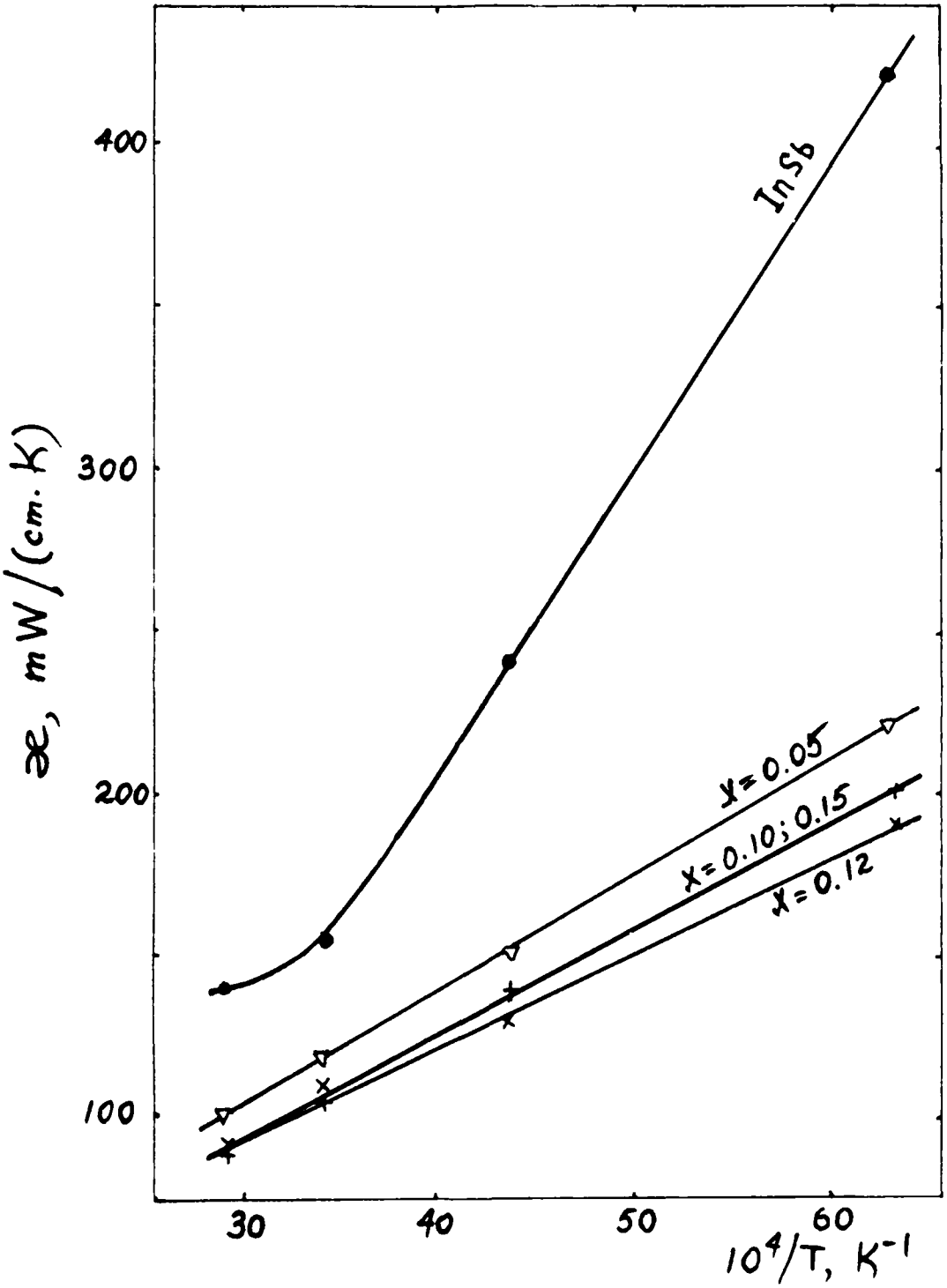

Figure 8. Temperature dependence of the thermal conductivity of $(HgTe)_x(InSb)_{1-x}$ single crystals.

10. GENERAL REVIEW

The principal objective of this project was demonstration of the new $(HgTe)_x(InSb)_{1-x}$ semiconductor materials' capability to combine the main merits of indium antimonide as an infrared detector material, namely, direct interband transition, extremely high electron mobility, and very high ratio of electron-to-hole mobilities [19], with the ability of the controllable and uniform adjustment of the cut-off wave length which comes from alloying of InSb with the semimetallic mercury telluride.

The preliminary consideration [20] gave us reason to conclude that the main advantages of the alloy system consist of some important technological features, namely, low liquidus and solidus temperatures, relatively high microhardness, and what was most attractive, slow change of the cut-off wave length with the alloy composition change. The results of investigation [20] led us to expect that the HgTe-InSb (IMAT) alloys will have substantial advantages as a material for far-infrared detectors before the mercury-cadmium tellurides (MCT), mercury-manganese tellurides, and mercury-zinc tellurides (MZT) from both physical and technological points of view.

This report includes the results of our third year work which consists of experimental correction of the phase diagram on the basis of the DTA on the single-crystalline samples, investigation of the electric, galvano-magnetic, and thermal properties of a

group of IMAT single crystals, and the most important part of our experiments, the preparation and investigation of the models of the IMAT far-infrared (FIR) detectors.

All results of the project are summarized to analyze the achievements of the work and to show the most effective directions of the following investigation of this new and, from our point of view, prospective group of narrow-band semiconductor compounds.

The interest toward the II-VI/III-V alloys is caused by the opportunities to find new combinations of the fundamental physico-chemical properties that may be prospective for practical use of this vast group of materials as well as for understanding the processes that take place in the multicomponent solids. At the moment we know 26 combinations of II-VI/III-V alloys which have been synthesized and investigated. These are ZnS with AlP [24], GaP [24-29], InP [24]; CdS with GaP [30], InP [30, 45], GaAs [30, 46], InAs [47]; ZnSe with GaP [24, 25, 30, 26, 50, 61, 63-65], InP [30], GaAs [26, 30, 40, 42, 44, 51-59]; CdSe with GaP [30]; InP [45], GaAs [30, 48], InAs [47, 49]; ZnTe with AlSb [30], GaP [30], GaAs [30, 52, 54]; CdTe with AlSb [28], GaAs [41, 43], InP [45], InAs [32, 34, 36-39, 72, 73], InSb [31, 33, 35, 38]; HgTe with GaSb [66, 67], InAs [67-69], InSb [16, 20, 70].

Transition from relatively simple elemental (Ge, Si) and binary (GaAs, InP, InSb, CdTe, etc.) tetrahedral semiconductors to more complicated ternary and quaternary materials meets substantial obstacles. The theory of these materials is so far almost

nonexistent and the lack of sufficient experimental results does not provide an opportunity for its development. Nevertheless, the progress made with transitions from the elemental to binary materials makes it evident that the multicomponent materials will provide opportunities for discovering new and unexpected combinations of properties of these materials which may in the future find a proper place among the scientifically and industrially useful semiconductors, and in certain cases even replace some of the existing electronic elements.

One of the practical problems which is unsolved even now is the problem of a suitable material for far-infrared detection in the range of both the atmospheric window 8-14 μm and the usually bolometric range 140-1200 μm. The most commonly used extrinsic semiconductors for bolometers are n-InSb [93-95] and n-GaAs [96]. More and more attention is being paid to n-$Hg_{1-x}Cd_xTe$ as a potentially useful alternative detector to InSb for FIR and short-millimeter wavelengths [23, 97-99]. The MCT use as an electron bolometer was first suggested back in 1965 [93]; nevertheless, even now the available MCT material is not suitable for a detector that has parameters comparable to InSb. The main problem with MCT single crystals is their axial and radial nonuniformity. For example (see [23]), the best crystals available to the authors (Mullard, Southampton, UK) had $\Delta x \cong 0.01$ on the distance 1.8 mm in the axial direction.

In the case of IMAT crystals, axial non-uniformity, as we found in our investigation of axial distribution of density of grown crystals, was substantially smaller than in MCT (smaller than $\Delta x = 0.01$ on the distance 20 mm along the growth axis in the central part of the crystal). A simple explanation is there is a relatively small difference in the melting points of InSb and HgTe in comparison with the difference between the melting points of HgTe and CdTe. Another disadvantage of MCT is the very strong dependence of its energy gap on composition in comparison with the IMAT alloys.

Our experiments show that the IMAT FIR detectors may be superior to n-InSb also. A limitation on InSb is the low electric field that can be applied before breakdown occurs. But, as was shown in Section 4 of this report, the breakdown electric field in IMAT is greater than in InSb. If we take into consideration some important advantages of IMAT over MCT, there is no doubt that IMAT appears to be more competitive than MCT as an alternative detector to InSb.

11. PROSPECTIVES OF THE FOLLOWING RESEARCH

Future work with the IMAT materials should be concentrated, first of all, on its technological side. Improvement of the PC detector parameters depends substantially on the capability of the growth of crystals with intrinsic carrier concentration of about 10^{14} cm^{-3}, whereas the obtained level is about 10^{16} cm^{-3}. Experiments on the interaction of IMAT alloys with dopants ought to be the starting point of investigating the alloys as material for the PV detectors. Work on the bulk crystals has to be parallel with the investigation of the process of thin epitaxial film growth and its optimization. Substantial progress in the area of the IMAT IR detectors, and especially arrays, may be reached if a technological process of epitaxial growth of the intrinsic IMAT films of about 20-30 μm thick has been developed with electrical and optical parameters of the films on the level of those of the bulk crystals. The composition of both crystals and epilayers for the detectors working in the atmospheric window range has to be near $x = 0.12$. From our point of view, one of the most effective methods of film growth is the photolytic and/or radiolytic MOVPE (see Appendix), because these methods provide an opportunity for the effectively controlled low temperature growth. Another technological development for the future is growth of multilayered HgTe/InSb structures for both IR detectors and for IR radiation sources. These

materials are especially promising for this purpose because their lattice parameters differ only by 0.2% with the same crystal structure.

The results of the investigation undertaken on the IMAT alloys provide information on their electrical and thermal transport properties, on interaction of incident IR photons with crystals, and to some extent, on the processes of ionization and recombination of the current carriers. But such characteristics of the material as elastic moduli, thermal expansion coefficient, parameters of phonon spectra, magnetic susceptibility, and some thermodynamic parameters still are waiting for their investigator. Some of the properties, such as thermal expansion coefficient and energy of formation, are important for the detector design and crystal (epilayer) growth. The other characteristics are important for understanding the nature of the forces of interatomic interaction in the IMAT crystal lattice, propagation of the phonons in it, etc., and may be considered as an addition to the information we possess regarding the multicomponent tetrahedral semiconductors.

Work in the area of the IMAT FIR detectors has to be directed toward optimization of the protective coating of the radiation absorbing surface of the detector, choice and investigation of the electric contacts and housing, and manufacturing and investigation of the FIR detector arrays for both PC and PV modes.

In conclusion, it is reasonable to mention once more that the work with this group of IR detector materials is at its very

initial stage, and it is difficult to foresee all possible directions of its development. Nevertheless, it is clear even now that these alloys will occupy an important place among prospective and useful infrared materials.

12. SUMMARY

The following lists the major accomplishments reached in the investigation of $(HgTe)_x(InSb)_{1-x}$ alloys.

- Liquidus and solidus temperature measurements were done on alloys; the T-x diagram for non-controllable pressure showed the existence of solid solutions, at least for alloys with $0 < x \leq 0.18$.
- The crystal structure and lattice constant of the crystals of solid solutions were measured as a function of the chemical composition.
- Bulk crystal growth methods were developed and a group of IMAT single crystals was grown with x magnitude equal to 0.05, 0.10, 0.12, and 0.15.
- Microhardness of the alloys was measured at room temperature; thermal conductivity was measured between 77K and 373K.
- Electrical transport properties of the alloys were measured on poly- and single crystals; the achieved charge carrier concentration was of the order of 10^{16} cm^{-3}; it was shown that the breakdown electric field strength in the IMAT alloys is substantially greater than in the InSb crystals; all single-crystalline samples had a conductivity of n-type.

- Optical transmission and reflection measurements showed that the semiconductor alloys in the system form a row of continuous solid solutions with $0 < x \leq 0.16$; the cutoff wavelength in this range of composition is changing from 6 to ~15 μm.
- Investigation of the detecting parameters on the detector models with $x = 0.10$ and $x = 0.12$ showed that detectivity has a magnitude of the order of 10^9 cm · $Hz^{1/2}$/W and the voltage photoresponse is of the order of 1 V/W at 77K for the wavelength 10.6 μm.
- The overall results indicate that the crystals investigated have certain electro-optical and technological advantages and thus there appear to be significant reasons to continue determinations of the remaining uncertain or unknown properties of these materials.

13. ACKNOWLEDGEMENTS

The authors, Dr. L. I. Berger and Dr. S. W. Lin, wish to thank Dr. L. J. Burnett, Chairman of the Physics Dept. of SDSU for the courteous opportunity to use department premises and equipment. We are grateful to Mr. R Steed for his help in optical measurements.

We express our appreciation to Dr. A. Clawson of Naval Ocean Systems Center for the opportunity of verifying our results of galvano-magnetic measurements on the NOSC equipment. We thank Mr. Peter Gantzel of General Atomic Technology, Inc., San Diego, for the Laue X-ray analysis of some of our single crystals. We would like to express our thanks to Mrs. M. L. Oliver for typing the report.

We are very grateful to the Office of Naval Research for the financial support which made this investigation possible, and especially to Dr. J. S. Murday and Dr. V. Nicolai for their permanent interest in this work.

14. REFERENCES

1. M. A. Kinch and S. R. Borello. Infrared Phys., 15, 11 (1975).
2. S. Borello, M. Kinch and D. LaMont. Infrared Phys., 17, 121 (1977).
3. V. Gopal and A. V. R. Warrier. Infrared Phys., 24, 387 (1984).
4. F. K. Neuman. Journ. Electrochem. Soc., 109, 345 (1962).
5. E. Z. Dziuba. Journ. Electrochem. Soc., 116, 104 (1969).
6. M. R. Lorenz and R. E. Halstead. Journ. Electrochem. Soc., 110, 343 (1963).
7. P. W. Kruse. Semiconductors and Semimetals. Ed. R. K. Willardson and A. C. Beer, Vol. 5, 1970, p. 15.
8. H. J. Hrostowski, G. H. Wheatley, and W. F. Flood, Phys. Rev., 95, 1963 (1954).
9. T. M. Lloyd. Thermal Imaging System. Plenum, N.Y., 1975, p. 11.
10. S. I. Novikova and N. K. Abrikosov [illegible] Solid State, 5, 1558 (1964).
11. T. Albert and G. A. Saunders [illegible] (1967).
12. P. Leroux-Hugon, N. [illegible] (1967), Collogue C1, [illegible]

13. R. H. Kingston. Detection of Optical and Infrared Radiation. Springer-Verlag, Berlin, N.Y., Lnd., 1978.

14. M. Levinstein. Semiconductors and Semimetals. Ed. R. K. Willardson and A. C. Beer, Vol. 5, 1970, p. 3.

15. R. L. Petritz. Proc. IRE, 47, 1458 (1959).

16. L. I. Berger and S. W. Lin. Quarternary Narrow-Band Semiconductors $(HgTe)_x(InSb)_{1-x}$ for Far-Infrared Detectors. Annual Report 1983-1984. ONR Grant N00014-83-K-0588.

17. R. J. Keyes and T. M. Quist. Semiconductors and Semimetals, Vol. 5, Academic Press, 1970, p. 321.

18. W. Shockley and W. T. Read. Phys. Rev., 87, 835 (1952).

19. T. S. Moss. Semiconductors and Semimetals, Vol. 2, Academic Press, 1966, p. 231.

20. L. I. Berger. Abstracts of the 5th Intern. Conf. on Vapor Growth and Epitaxy. Coronado, California, 1981, p. 331.

21. M. Rodot. Les Materiaux Semiconducteurs. Dunod, Paris, 1965.

22. E. M. Barrall. Thermochim. Acta, 5, 377 (1973).

23. M. F. Kimmitt, G. C. Lopez, J. C. Giles, M. Takai, H. P. Roser, B. T. McGuckin and A. Black. Infrared Phys., 25, 767 (1985).

24. A. Addamiano. J. Electrochem. Soc., 107, 1006 (1960).

25. I. Bertoti, E. Barta, J. Schanda, and P. Sviszt. Proc. Int. Conf. Luminescence, Budapest, 1966, p. 1102.

26. W. M. Yim. J. Appl. Phys., 40, 2617 (1969).

27. A. Shintani and S. Minagawa. J. Phys. Chem. Solids, 34, 911 (1973).

28. H. Sonomura, T. Uragaki, and T. Miyauchi. Japan J. Appl. Phys., 12, 968 (1973).

29. V. S. Blashkiv, G. M. Grigorovich, L. B. Panchenko, P. N. Tkachuk, and V. S. Manzhara. Sov. Phys. Semicond., 17, 353 (1983).

30. W. M. Yim, J. P. Dismukes, and H. Kressel. RCA Rev., 31, 661 (1970).

31. A. L. Petrov. Sov. Phys. Semicond., 15, 339 (1981).

32. A. D. Stuckes and R. P. Chasmar. J. Phys. Chem Solids, 25, 469 (1964).

33. L. A. Skorobogatova, A. L. Petrov, and G. A. Kuzmina. Sov. Phys. Semicond., 13, 480 (1979).

34. A. V. Voitsekhovskii and V. P. Drobyazko. Inorg. Materials, 3, 1976 (1967).

35. L. A. Skorobogatova and E. N. Khabarov. Sov. Phys. Semicond., 8, 257 (1974).

36. N. A. Semikolenova and E. N. Khabarov. Sov. Phys. J. (USA), 16, 801, 807 (1973); Izv. VUZ Fiz. USSR, 16, 76, 82 (1973).

37. A. L. Petrov and G. A. Kuzmina. Sov. Phys. Semicond., 14, 604 (1980).

38. G. I. Buzevich, L. A. Skorobogatova, and E. N. Khabarov. Sov. Phys. Semicond., 7, 1389 (1974).

39. V. N. Morozov, A. L. Petrov, and L. A. Skorobogatova. Sov. Phys. Semicond. 11, 1192 (1977).

40. A. V. Voitsekhovskii, N. G. Vyalyi, Y. P. Drozhzhov, and M. V. Chukichev. Sov. Phys. Semicond., 12, 1431 (1978).

41. V. A. Anishchenkko, A. V. Voitsekhovskii, and V. E. Sharenko. Ukr. Fiz. Zh (USSR), 18, 1735 (1973).

42. A. V. Voitsekhovski, N. G. Vyalyi, and A. D. Pashun. Inorg. Materials, 16, 1909 (1980).

43. V. A. Anishchenko, A. V. Voitsekhovskii, and A. D. Pashun. Sov. Phys. Semicond., 13, 850 (1979).

44. P. N. Tkachuk, V. S. Blashkiv, G. M. Grigorovich, and V. S. Manzhara. Zh. Prikl. Spektrosk., 33, 1049 (1980).

45. N. A. Goryunova and V. I. Sokolova. Izv. Moldav. filiala ANSSR, 3, 31 (1960).

46. V. N. Astakhov, N. G. Vyalyi, and A. D. Pashun. Naukovy Trudy Ukr. Silskogospod. Akad., 238, 91 (1980).

47. A. V. Voitsekhovskii, V. P. Drobyazko, V. K. Mityurev, and V. P. Vasilenko. Inorg. Materials, 4, 1681 (1968).

48. A. V. Voitsckhovskii and A. D. Pashun. Ukr. Fiz. Zh. (USSR), 18, 1558 (1973).

49. V. P. Drobyazko. Sov. Phys. Semicond., 12, 354 (1978).

50. A. V. Voitsekhovskii, V. N. Krupa. T. P. Stetsenko, and V. V. Chernyi. Fiz. Kondensir. Sostoyaniya, Kiev, 1980, p. 44.

51. E. G. Shevchenko, L. M. Dolginov, F. A. Gimelfarb, K. K. Dubenskii, and L. A. Zhukova. Inorg. Materials, 9, 31 (1973).

52. R. Hill. Thin Solid Films, 27, L1 (1975).

53. N. A. Borisov, V. M. Lakeenkov, M. G. Milvidskii, and O. V. Pelevin. Sov. Phys. Semicond. 10, 948 (1976).

54. R. Hill. Thin Solid Films, 34, 395 (1976).

55. V. N. Astakhov, A. V. Voitsekhovskii, N. G. Vyalyi, and V. V. Chepelev. Ukr. Fiz. Zh. (USSR), 22, 230 (1977).

56. N. A. Goryunova and N. N. Fedorova. Sov. Phys. Solid State, 1, 307 (1959).

57. V. M. Lakeenkov, L. M. Morgulis, M. G. Milvidskii, and O. M. Pelevin. Inorg. Materials, 13, 1517 (1977).

58. S. M. Ku and L. J. Bodi. J. Phys. Chem. Solids, 29, 2077 (1968).

59. A. I. Chernyshov, G. M. Zeleva, and I. A. Kirovskaya. Inorg. Materials, 14, 1020 (1978).

60. A. Shintani and S. Minagava. J. Phys. Chem. Solids, 34, 911 (1973).

61. H. Sonomura, T. Uragaki, and T. Miyauchi. Japan J. Appl. Phys., 12, 968 (1973).

62. V. S. Blashkiv, G. M. Grigorovich, L. B. Panchenko, P. N. Tkachuk, and V. S. Manzhara. Sov. Phys. Semicond., 17, 353 (1983).

63. O. V. Bogdankevich, N. A. Borisov, B. M. Lavrushin, V. V. Lebedev, A. G. Negodov, and S. S. Strelchenko. Sov. J. Quant. Electron, 2, 138 (1972).

64. P. W. Yu and M. Glicksman. J. Appl. Phys., 43, 4153 (1972).

65. A. Catalano, R. Beaulieu, T. Gregg, P. Head, A. Wold, and M. Glicksman. Solid State Commun., 14, 421 (1974).

66. V. P. Ambros and I. I. Burdian. Abstracts of the 1968 Conf. Tiraspol Pedagogical Institute, Tiraspol, MSSR, 1968, p. 38.

67. N. A. Goryunova. "Slozhnye Almazopodobnye Poluprovodniki" (Multicomponent Diamond-like Semiconductors). Sov. Radio Publ. House, Moscow, 1968, p. 224.

68. L. A. Osnach. "Investigations in Mathematical and Experimental Physics," Proc. LISI, Leningrad, 1965, p. 36.

69. Y. L. Berger and L. I. Berger. Bull Amer. Phys. Soc., 31(3), 560JU10 (1986).

70. J. A. Rios, S. W. Lin, and L. I. Berger, ibid., 31(3), 399EU8, (1986); S. W. Lin and L. I. Berger, ibid., 31(3), 560JU8 (1986).

71. A. Inyutkin, E. Kolosov, L. Osnach, V. Khabarova, E. Khabarov, and P. Sharavskii. Izv. Akad. Nauk USSR, Fizika, 28, 1010 (1964).

72. G. I. Bazhenova, E. A. Balagurova, A. A. Ryazantsev, and E. N. Khabarov. Inorg. Materials, 10, 1770 (1974).

73. V. N. Morozov and V. G. Chernov. Inorg. Materials, 15, 1036 (1979).

74. L. S. Palatnik, Y. F. Komnik, and V. M. Koshkin. Kristallografiya, 7, 563 (1962) (Russian).

75. H. R. Huff, H. Kraus, and B. M. Brazeale. Proc. IRIS Spec. Group on IR Detection, July 1974, p. 77.

76. W. F. H. Micklethwaite and R. F. Redden. Appl. Phys. Lett., 36, 379 (1980).

77. P. M. Raccah, U. Lee, J. A. Silberman, W. E. Spicer, and J. A. Wilson. Appl. Phys. Lett., 42, 374 (1983).

78. G. Nimtz, B. Schlicht, and R. Dornhaus. Appl. Phys. Lett., 34, 490 (1979).

79. T. A. Shakhnazarov. Inorg. Materials, 15, 56 (1979).

80. F. A. Zaitov, L. A. Bovina, and V. A. Stafeev. Problemy Fiziki Soedinenii A B . Mat. Vsesoyuz. Soveshch., 1972, p. 3 (Russian).

81. L. B. Valdes. Proc. IRE, 42, 420 (1954).

82. D. Shaw. Phys. Status Solidi, A89, 173 (1985).

83. I. B. Mizetskaya, V. N. Tomashik, and P. F. Vengel. Inorg. Materials, 19, 914 (1983).

84. C. A. Wang, A. F. Witt, and J. R. Carruthers. J. Crystal Growth, 66, 299 (1984).

85. K. Seeger. Semiconductor Physics, 3rd Edition, Springer-Verlag, New York, 1985.

86. R. F. Potter. Bull. Am. Phys. Soc., 1, 53 (1956).

87. L. J. Slutsky and C. W. Garland. Phys. Rev., 113, 168 (1959).

88. T. Alper and G. A. Saunders. J. Phys. Chem. Solids, 28, 1637 (1967).

89. J. G. Mavroides and D. F. Kolesar. Solid State Commun., 2, 363 (1964).

90. H. Ehrenreich. J. Phys. Chem. Solids, 12, 97 (1959).

91. H. Weiss. Zs. Naturforsch, 11a, 430 (1956).

92. W. D. Lawson, S. Nielsen, E. H. Putley, and A. S. Young. J. Phys. Chem. Solids, 9, 325 (1959).

93. E. H. Putley. Semiconductors and Semimetals, Vol. 1, Chapter 3, Academic Press, N.Y., 1966.

94. E. M. Putley, ibid., Vol. 11, Chapter 3, 1977.

95. T. G. Phillips and K. B. Jefferts. Rev. Sci. Instr., 44, 1009 (1973).

96. G. E. Stillman, S. M. Wolfe, and J. O. Dimmock; ibid., Chapter 4 (1977).

97. J. W. V. Storey. Infrared Phys., 25, 583 (1985).

98. B. A. Weber and S. M. Kulpa. Japan J. Appl. Phys., 19 (Suppl. 19-3), 345 (1980).

99. B. A. Weber and S. M. Kulpa. Int. J. Infrared Millimeter Waves, 3, 235 (1982).

100. J. L. Schmit and E. L. Stelzer. J. Electron. Materials, 1, 65 (1978).

101. E. O. Kane. J. Phys. Chem. Solids, 1, 249 (1957).

102. Excitons. Topics Current Physics. Ed. K. Cho, Vol. 14, Springer, 1979.

103. M. D. Sturge. Phys. Rev., 127, 768 (1962).

104. H. J. Hrostowski, G. H. Wheatley, and W. F. Flood. Phys. Rev., 95, 1683 (1965).

15. APPENDIX: ON MOVPE OF CMT AND IMAT ALLOYS

The epitaxial growth of semiconductor films utilizing metal-organic compound has become important in several semiconductor device fields. At the present time, there is information that the method has been applied to the fabrication of field-effect transistors, Gunn device, high speed heterojunction bipolar transistors, high efficiency photocathodes, solar cells, high performance double heterostructure lasers, etc.

There can be no doubt that the MOVPE may be effectively used in the fabrication of IR detectors, and especially IR arrays, because of some inherent characteristics of the basic chemical reactions governing the formation of the epitaxial layer, the possibility of the process to be well controlled and simplicity of the doping process. The process appears to be easiest of the available epitaxial technologies.

Nevertheless, there are only a few publications (mainly by a group of English authors) devoted to the process of MOVPE of infrared materials, to be certain, only of MCT, and there is no available information on the use of MOVPE for IMAT. Hence, the use of MOVPE for the growth of IMAT alloy layers is a completely new step in the field of semiconductor materials for IR detectors. These materials will have significantly improved optical and electro-optical parameters, namely, (i) photo-response time, by use

of the binary compounds with the highest known mobility and the smallest effective mass of free charge carriers; (ii) cut-off wavelength resolution, by using semiconductor solid solutions with relatively small composition dependence of energy gap; and (iii) detector long-term stability, as a result of the relatively small change in electro-optical properties with a change of composition due to sublimation of the volatile components from the surface of the epitaxial layer (in contrast to MCT).

The main objective of our work is growth of the epitaxial layers of semiconductor solid solutions for far-infrared detectors with the improved optical and electro-optical parameters. To achieve this objective, the new method of epitaxial growth--the metal-organic chemical vapor deposition--may be developed and adjusted for the layers of solid solutions $(HgTe)_x(InSb)_{1-x}$. Photolytic and a completely new radiolytic process of the metal-organic compound's decomposition may be used for IR detectors and IR arrays material preparation.

The specific detectivity of a semiconductor IR detector depends directly upon the noise level in the active medium of the detector. The noise level depends substantially upon the nature and concentration of the defects in the crystal or the layer of semiconductor material of the detector.

In the crystals and thin layers of MCT, as an interesting and relatively new material for IR detectors, the critical role belongs to the point defects, mainly the Hg vacancies. High partial

pressure of mercury causes Hg sublimation from the surface of MCT and diffusion of vacancies in the volume and along the surface of an MCT crystal or layer. The higher the temperature in the process of material preparation, the greater is the probability of the composition nonuniformity and resulting diffusion, sublimation and consequent change of the detector parameters.

The MOVPE takes place at comparatively low temperatures in the pyrolytic process and may even be done at temperatures below 0°C in the photolytic process. It is reasonable to expect, in accordance with literature data, that the MOVPE process will provide MCT material for IR detectors and especially for arrays with better electro-optical parameters and their uniformity, as well as with better long-term stability in comparison with MCT crystals and layers grown by convenient bulk and epitaxial layer technology. The use of MOVPE for IMAT layer fabrication may be also extremely promising, as it was proved, for example, in the case of such an important electro-optical material as the quaternary alloys GaAs-InP.

The basis for the material fabrication method is founded upon the fact that the epitaxial growth of compound semiconductors utilizing metal-organics has become important in several device fields. During the last 15 years, MOCVD has been used in some high performance electronic and optoelectronic devices. The advantages of MOVPE include the use of a single hot area for deposition in the process of pyrolysis and growth, or the total absence of a heated

area in the case of photolytic and radiolytic MOVPE. Also, the process is halide-free and in many cases an etching-free one.

In the case of multi-component epitaxial layers, MOVPE has especially important advantages over bulk methods because growing images of IMAT, as well as MCT, have to contend with a high Hg partial pressure and large segregation effects due to a wide separation between the liquidus and solidus curves.

Conventional epitaxial growth techniques also have some disadvantages in comparison with MOVPE. A close-spaced sublimation technique for MCT growth on a CdTe substrate can result in a large interdiffusion region and uncertain layer composition. The use of an open flow system based on hydrogen transport of the elements enabled growth of MCT over a wide composition range, but control of composition is very difficult. Low temperature growth of MCT by vacuum deposition reduces the interdiffusion between an epitaxial layer of MCT and CdTe substrate, but growth rate is too low for practical use. LPE of MCT from a Te rich solution gives poor layer quality for Cd content less than 0.3, which is the important composition range for ID detectors. Also, growth temperatures are relatively high and interdiffusion between layer and substrate can be a problem. Growth of MCT by LPE from Hg rich solutions requires high Hg partial pressure and results, in general, in varying composition during growth.

The scientific basis for the choice of the IMAT for MOVPE growth is founded upon the fact that InSb, which has a maximum IR

sensitivity at about 6 μm, possesses the highest carrier mobility among all known semiconductors (up to 10^6 cm^2/V sec; cf. with CdTe - 10^2 - 10^2 cm/V sec). HgTe, in turn, also has relatively high carrier mobility (about 7×10^4 cm/V sec). Solid solutions of HgTe and InSb must exhibit better photo-response characteristics than any other combination, including the well-known $Hg_xCd_{1-x}Te$ crystals and films. HgTe and InSb have much closer melting points--670°C and 536°C, respectively--and lattice constants--6.462 and 6.479A, respectively, in comparison with HgTe and CdTe (670°C and 1041°C, and 6.462 and 6.482A, respectively). This means that detector-quality crystals of $(HgTe)_x(InSb)_{1-x}$ can be grown with fewer difficulties and with higher yield than that of HgCdTe. In fact, solidus temperatures in the system HgTe-InSb are lower than the melting point of HgTe, and the vapor pressure over the melt of HgTe-InSb is essentially lower in comparison with the melt of a "standard" material, $Hg_{.8}Cd_{.2}Te$.

Furthermore, the present low yield of detector-quality HgCdTe crystals (about 10%) is conditioned mainly by the high HgTe concentration (up to 80%) and the high process temperature. These are required by the large energy gap (1.44-1.56eV) and high melting point of CdTe. Crystals of $(HgTe)_x(InSb)_{1-x}$ with the same optical parameters (energy gap about 0.10eV), have HgTe concentrations of not more than 15% and much lower solidus temperatures.

The most important advantage of HgTe-InSb crystals in IR detectors results from the fact that the difference between energy

gaps in the binary components (0.47eV) is much smaller than the system $Hg_xCd_{1-x}Te$ (1.9eV). This means that non-uniformity of composition in the quaternary materials will not strongly change the cut-off wavelength distribution along the crystal. This is especially important for IR arrays. The concentration cut-off wavelength shift near to the wavelength 12.5 μm is equal to 2.1 μm/percent for HgCdTe and only 0.6 μm/percent for HgTeInSb.

A brief review of data on MCT is necessary because it is an important group of materials used now for infrared applications ([1] in the following list of references). The alloys are an intrinsic detector material and the energy gap of them varies in the range 0.1.6eV with composition of HgTe and CdTe. The $Hg_{0.8}Cd_{0.2}Te$ alloy is especially useful for the 8-14 μm atmospheric transmission window. Because of its intrinsic property, the MCT detector operates with higher detectivity at a higher temperature than the usual extrinsic detector materials such as doped Ge and doped Si. High-performance detectors are made of n-type material with a carrier concentration in the range 10^{14}-10^{15} cm^{-3} and bulk lifetime limited by Auger process.

However, MCT is a notoriously difficult material to prepare from the melt because of the high Hg vapor pressure that is generated at its liquidus temperature. This pressure can be about 35 atm [2, 3]. Crystal growth methods of MCT and detector performances have been reported in [4, 5]. The modified zone melting method was first reported by the authors [6].

MCT can be grown from the vapor phase by depositing a layer of HgTe onto a substrate of CdTe and subsequently carrying out an interdiffusion by heat treatment [7-12]. There is also information on LPE growth of MCT from Te-rich and Hg-rich solutions [13-15]. As mentioned above, the bulk methods for growing MCT are high pressure methods, and large segregation takes place because of a wide separation of solidus and liquidus curves in the quasibinary system HgTe-CdTe. Conventional VPE and LPE growth techniques also have some disadvantages; first of all, high temperatures that result in uncertain layer composition, larger interdiffusion region (for the close-spaced vapor transport), difficulties in the composition control, low growth rates, high partial pressure of Hg, difficulties in growth of n-type material, etc. Since the concept of the epitaxial growth of semiconductor compounds by MOCVD method [16] and the first successful attempts of its use for the group of zinc-blend structure binary compounds [17-23] were published, the epitaxial growth of multicomponent semiconductors has become important in several device fields.

The MOCVD method has several important advantages. In its most general interpretation, it can refer to the deposition of multiconstituent films using decomposition of any of several metal-organic compounds for the source of one of the constituents. In the MOVPE process, film constituents are transported to the reaction zone in the form of gaseous metal-organics. In the reaction zone they undergo decomposition and metallic components

deposit on the proper substrate. Sometimes hydrides of some constituents, or even metallic vapors, participate in formation of the growing layer. It is evident that the gaseous nature of the reactants and usual simplicity of reactions identify MOVPE as a useful epitaxial technology. The process can be well controlled by fixing the flow rates, and thus the partial pressure of the various reactants. Complex multilayer epitaxial structures are readily formed by exchanging one gas composition for another. The pyrolytic reaction requires that only the substrate be heated to ensure efficient decomposition. The photolytic reaction apparently may be even more convenient for the epitaxial growth process control. Finally, the process is simply adjustable to mass production.

However, the MOVPE process has some disadvantages which have to be taken into consideration. As mentioned before, a number of metal-organic compounds, including most widely used alkyls, have a tendency to react at room temperature with each other and with hydrides [22] to form simple or polymeric adducts. As a result, the adducts typically collect on the reactor walls, and this drastically alters the growth rate and possibly the composition of the grown material. So far, there are difficulties in the achievement of uniform crystal growth, both in horizontal and vertical reactors. Our future goal is familiarization of the MOVPE method for the growth of IMAT epitaxial layers, using pyrolytic, photolytic and/or radiolytic techniques.

Information on MOCVD of II-VI semiconductors and their solid solutions was first presented in [23-26]. First layers of $Cd_xHg_{1-x}Te$ with $0 \leq x \leq 0.5$ were grown from metal-organics by authors [27]. In their work, vapors of $(CH_3)_2Cd$ and $(C_2H_5)_2Te$ (DMCd and DETe respectively) were transported in H gas and flow of Hg vapor. The growth of MCT layers was carried out at 410°C. The growth rate of the layers was about 10 μm/h for x = 0.2. It was possible to grow layers of controlled composition by controlling the flow of DMCd. All specimens but one were n-type with $n = 10^{16} - 10^{18}$ cm^{-3}. The magnitude of mobility was from $\mu = 10^5$ to $\mu = 2.4 \times 10^3$ $cm^2/V \cdot s$ for x = 0.14 and for x = 0.25 respectively at 77K. In their next publication [28] the authors showed a very strong dependence of the layer composition on temperature change from ~425°C to ~410°C. The authors explain the results taking into consideration a suggestion on the preferential pyrolysis of DETe in the presence of DMCd. No attempt was made to consider the influence of the ambient pressure and hydrodynamic parameters of the reactor including Reynolds' number in the deposition chamber.

The authors [29] present the magnitude of μ and n of about the same range. The only important difference is that the growth rate was about 6 μm/h. X-ray fluorescence experiments showed the excellent compositional uniformity through a $Hg_{0.85}Cd_{0.15}Te$ layer (Fig. 1).

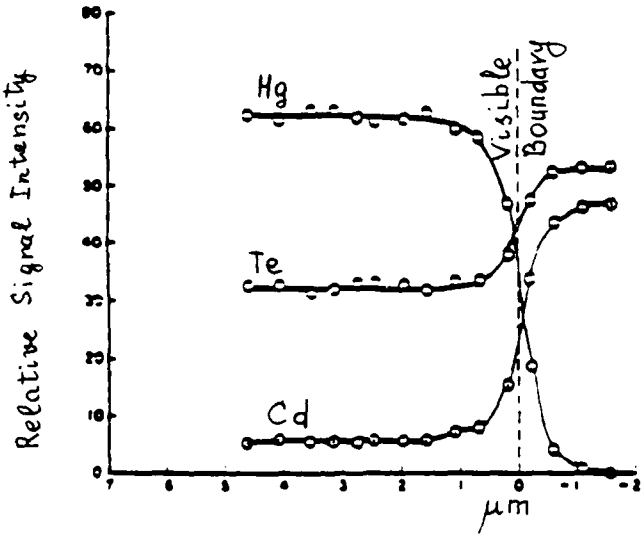

Figure 1. Compositional uniformity through a Hg0.85Cd0.15Te layer as determined by X-ray fluorescence [29].

There are very few publications on MOVPE growth of MCT, and not one of them gives exhaustive information about important features of the process. These questions are first of all:

1. Is the flux of the gas phase components a laminar or turbulent one?
2. What is the actual ratio of the metal component concentrations upon the substrate?
3. What is the magnitude of viscosity of the vapor phase components and its temperature dependence?
4. Is there a dependence of the growth parameters (growth rate, defect density, layer composition, thickness, uniformity, surface morphology, etc.) on Reynolds' number(s)?
5. Is there a correlation between the ambient atmospheric pressure and the growth parameters?
6. Is there any definite correlation between the substrate geometry, orientation, and the location of it in the reactor and the growth parameters?
7. Is there a correlation between the growth parameters and design of the reactor exhaust part and burner as well as the burning process?

All known results of the MCT MOVPE have been determined by the pyrolytic cracking process of the metal alkyes upon a heated substrate, usually CdTe [31, 39]. But at the elevated temperature of

the substrate, an elevated mercury partial pressure is required to exceed the equilibrium pressure of Hg over the growing MCT layer [32]. Thus, there are definite limitations to the independent variables of the MOVPE process. Besides, the optimal cracking temperatures for metal alkyls are different, and quite often the chosen substrate temperature is simply a lesser evil. An alternative to this is the use of ultraviolet photon flux for the metal alkyl cracking in combination with (or without) a controlled temperature of the substrate. Using photolytic reactions in combination with pyrolytic one may independently control two main parameters of the decomposition process: growth rate and the growing layer composition.

Experiments in the field of photolytic MOVPE HgCdTe may give information on the mechanisms of photochemical reactions.

As is known from the photolysis theory [33-38], the best expression for a photochemical reaction is

$$K = \frac{1}{N_m} \cdot \frac{dN_m}{dt} = a\gamma \cdot \frac{I_o}{hf} \qquad (1)$$

where K is the reaction constant, N is concentration of the excited molecules, a--molecular absorption coefficient, γ is probability of an excited molecule to joining the reaction, I is intensity of the incident photon flux, and hf is the photon energy.

Using equation (1) on the basis of the postulate of Grotthus and Einstein's photochemistry law, it is possible to describe the

kinetics of the cracking process of metal alkyl molecules. It is reasonable to expect that this process will not follow Bunsen-Roscoe's law ($K \propto I_0$), but the first photon absorption transfers the molecule into a metastable state, and absorption of the second photon transfers the molecule from the metastable to the photochemically active excited state with the following cracking process. For this process $K \propto I_0^2$, but there is the possibility of a chain reaction with photochemical origination, especially at elevated temperatures. In this case, $K \propto (I_0/A)^{1/2}$ where A is a dimensional parameter (length, surface, etc.) [36-38].

Combining photolytic process with the thermal excitation process it is possible to describe the cracking-deposition process, first of all, from analysis of $K = f(I_0)$ curves in combination with the quantum yield and growth parameters measurements.

As is obvious, the temperature is not at all a critical parameter for a photolytic process of MCT deposition. It means, in principle, that the MCT solid solution epitaxial deposition can be undertaken not only from the gaseous metal-organic compounds, but also from those in liquid state (properties of some metal-organic compounds see in Table 1 [41, 42]).

Of special interest is the possibility of use of penetrating radiation (X-rays, gamma radiation) for the photolytic decomposition of metal-organic compounds. In this case, in principle, radiation photons may bombard the metal-organic molecules in the layer that directly adjoins the substrate.

TABLE 1. SOME PROPERTIES OF A GROUP OF METALORGANIC COMPOUNDS [41, 42]

Compound mol. wt.	Dimethyl Cd 142.5	Dimethyl Hg 230.7	Diethyl Te 186	Triethyl In 202	Trimethyl Sb 167
Room temperature phase	Clear liquid	Clear liquid	Yellow liquid	Clear liquid	Clear liquid
Boiling point (°C at 760 mm)	105.5°	96°	137°	184°	80.6°
Melting point, °C	-4.5°	--	--	-32°	-87.6°
Specific gravity, gramm/cm^3	1.985	3.069	1.599	1.260	1.528
H_2O solubility	Decomp.	Insol.	Insol.	Decomp.	Sl. soluble
Vapor pressure, torr, at 0°C	9.7	18.84	2.1	1.35×10^{-2}	29.4
Vapor pressure, torr, at 20°C	28	50.17	7.0	4.97×10^{-2}	78.6
Vapor pressure, torr, at T°C	350 at 80°C	--	12.1 at 30°C	3.0 at 53°C 12 at 83°C	107 at 23°C
Vapor pressure vs. T°C, torr.	$10^{(7.764-\frac{1850}{T})}$	$10^{(7.575-\frac{1720}{T})}$	$10^{(7.99-\frac{2093}{T})}$	$10^{(7.409-\frac{2260}{T})}$	$10^{(7.728-\frac{1709}{T})}$

Unfortunately, the amount of publications devoted to the photolysis of metal-organic compounds, especially with the purpose of the following deposition of metal atoms on a substrate, is somewhat limited (see, for example, 43, 44). There are no data on the energy of metal-radical bond and its dependence on temperature, threshold wavelength of photolysis in gaseous and liquid state for the alkyls of interest, effect of temperature, ambient medium composition, and partial pressure on the sorption process of depositing atoms.

Nevertheless, from our point of view, photolytic MOVPE is a process that is apparently one of the most suitable for a programmed automatized production of the detector materials. Photochemical deposition (see [44]) offers an elegant solution to dissociate metal-organic on the substrate. Photolysis removes the dependence of deposition rate on substrate temperature [25]. The strong UV absorption for a number of Hg, Te and Cd alkyls and photolysis occur between 200 and 250 nm. The magnitude of growth rate usually is close to 1.5-2 μm/h [43] for HgTe at temperatures between 300 and 200°C. Apparently, the free mercury in the gas phase participate in a photosensitized reaction of the form

$$Hg^* + (C_2H_5)_2Te \rightleftarrows HgTe + 2C_2H_5$$

$$H_2 + 2C_2H_5 \rightleftarrows 2C_2H_6$$

We believe that use of metal-organics with mercury vapor will give opportunity for HgTe photolytic deposition at temperature close to 300K.

The radiolysis of metal-organics of Hg, Te, In and Sb is a completely new and potentially promising MOVPE technique. The advantage of this technique before the pyrolytic process is low temperature of decomposition and epitaxial growth. The advantage of radiolysis before photolytic process is the opportunity to have the source of radiation in the direct closeness with the surface of deposition. This means that the process of metal-organic decomposition will take place in the part of the reaction volume nearest to the surface of the substrate.

It is known (see, for example, [45, 46]) that a fast charged particle, moving through a medium, creates ionization, excitation, dissociation, and dissociative ionization of molecules. With any type of the initial fast particle, substantial part of chemical transformations of molecules is caused by their interaction with the secondary electrons of energy 101-103eV (mainly, Compton electrons).

In our planned work we are going to use as a source of initial radiation the isotope Sr^{90}. In accordance with [47], Sr^{90} has a lifetime 28.1 years with β^- - decay:

$$Sr^{90} \rightarrow Y^{90} + (\beta^-;\ 0.546\ \text{MeV}).$$

Y^{90} is a radioactive isotope with lifetime 64h and following reaction

$$Y^{90} \rightarrow Zr^{90} + (\beta^-;\ 2{,}273\ \text{MeV})$$

Energy in parenthesis is that of β^- particles. In our experiments with radiolytic MOVPE we shall put the plate containing Sr^{90} under the substrate of InSb (or any other). The plate will be surrounded by a screen that provides the motion of the primary and/or secondary electron in the part of the system containing gas stream of Hg, Te, In and Sb alkyls only through the substrate. Thus, the most intensive process of radiolysis of the alkyls will take place near the substrate surface. The electron flux will be regulated by an absorbing filter between the source of radiation and internal surface of the substrate or by an electric field between the source and substrate.

We expect that interaction of penetrating particles with the substrate lattice will play a role similar to that of heat motion of the substrate atoms at the elevated temperatures, while the substrate will be at room temperature or close to it. Some data regarding the materials are in Table 2.

In one type of the beta emitters [48] the active material (Sr^{90}/Y^{90}) is uniformly distributed over the surface of a 24 mm diameter stainless steel planchet and sealed in an aluminum mounting ring under a 0.9 mg/cm Mylar window. Special absorbers may be

TABLE 2. SOME PROPERTIES OF THE ISOTOPES [47, 48]

Parameter	Isotope	
	Sr^{90}_{38}	Y^{90}_{39}
Lifetime	28.1 year	64 h
Mode of decay	β^-	β^-
Decay energy, MeV	0.546	2.273
Particle energy, MeV (maximum)	0.546	2.273
Particle intensity, %	100	100
Thermal neutron capture cross-section	0.9 ± 0.5	--
Window, mg/cm^2	0.9	0.9
Price schedule, $ per 5 μCi	125	
(1982) 0.1 μCi	150	
1 μCi	225	
10 μCi	275	

included under the window to filter undesirable low energy radiation.

Summarizing, we have found that (1) MOVPE is a very promising method of the infrared material fabrication, (2) use of photolytic as well as radiolytic variations of MOVPE may open new possibilities in both the high quality epitaxial layer fabrication and understanding the mechanisms of decomposition reaction and the metallic atoms deposition, and (3) the MOCVD of HgTe-InSb quaternary alloys may become a new important achievement in the field of infrared detection, especially for the far-IR part of the spectrum.

References

1. R. Dornhaus and G. Nimtz. Springer Tracts Mod. Phys., 78, (1976).

2. R. F. Brebrick, A. J. Strauss. J. Phys. Chem. Solids, 26, 989 (1965).

3. J. Steininger. J. Electron. Mater., 5, 299 (1976).

4. E. L. Stelzer, J. L. Schmit and O. N. Tufte. IEEE Trans. Electronic Devices, ED-16, 880 (1969).

5. M. A. Kinch, S. R. Borello, and A. Simmons. Infrared Phys., 15, 111 (1975); 17, 127 (1977).

6. R. Ueda, O. Otsuki, H. Sinohara, and Y. Ueda. I. Crystal Growth, 13-14, 668 (19720.

7. F. Bailley, L. Svob, G. Cohen-Solal, and R. Triboulet. J. Appl. Phys., 46, 4244 (1975).

8. L. Svob, Y. Margaing, R. Triboulet, F. Bailley, and G. Cohen-Solal. J. Appl. Phys., 46, 4251 (1975).

9. O. N. Tufte and E. L. Stelzer. J. Appl. Phys., 40, 4559 (1969).

10. J. Saraie, S. Furukawa, B. Sawa, and T. Tanaka. Japan J. Appl. Phys., 12, 1259 (1973).

11. J. M. Pawlikowski. Thin Solid Films, 44, 305 (1977).

12. A. Piotrowska and E. Mizera, ibid., 44, 305 (1977).

13. T. C. Harman. J. Electron. Mater., 9, 945 (1980).

14. C. C. Wang, S. H. Shin, M. Chu, M. Lanir and A. M. B. Vanderwyck. J. Electrochem. Soc., 127, 175 (1980).

15. J. E. Bowers, J. L. Schmit, C. J. Speerschneider, and R. B. Maciolek. IEE Trans. Electron Device, ED-27, 24 (1980).

16. R. E. Ruhrwein. U.S. Patent 3,364,084; 1968.

17. H. M. Manasevit. Appl. Phys. Lett., 12, 156 (1958).

18. H. M. Manasevit and W. I. Simpson. J. Electrochem. Soc., 116, 1725 (1969).

19. H. M. Manasevit, ibid., 118, 647 (1971).

20. H. M. Manasevit, F. M. Erdmann, and W. I. Simpson, ibid., 118, 1864 (1969).

21. H. M. Mansevit and W. I. Simpson, ibid., 118, C291 (1971); 120, 135 (1973); 118, 664 (1971); 122, 444 (1975).

22. K. W. Benz, H. Renz, T. Weidlein, and M. H. Pilkuhn. J. Electron. Mater., 10, 185 (1981).

23. H. M. Manasevit and W. I. Simpson. J. Electrochem. Soc., 118, 644 (1971).

24. W. Stutius. Appl. Phys. Lett., 33, 656 (1978).

25. J. B. Mullin, S. J. C. Irvine, and D. J. Aschen. J. Cryst. Growth, 55, 92 (1981).

26. S. J. C. Irvine and J. B. Mullin. J. Cryst. Growth, 55, 107 (1981).

27. J. B. Mullin and S. J. C. Irvine. J. Phys. D.: Appl. Phys., 14, L149 (1981).

28. J. B. Mullin and S. J. C. Irvine. J. Vac. Sci. Technol., 21, 178 (1982).

29. W. E. Hoke and R. Traczewzki. J. Appl. Phys., 54, 5087 (1983).

30. S. J. C. Irvine, J. B. Mullin, and A. Royle. J. Cryst. Growth, 57, 15 (1982).

31. T. F. Kuech and J. O. McCaldin. J. Electrochem. Soc., 128, 1142 (1981).

32. C. L. Jones, M. J. Quelch, P. Capper, and J. J. Gosney. J. Appl. Phys., 53, 9080 (1982).

33. W. A. Noyes and P. A. Leighton. "The Photochemistry of Gases." Reinhold, N.Y., 1941.

34. G. M. Burnett and H. W. Melville in "Technique of Organic Chemistry." Ed. S. L. Friess and A. Weissberger. Intersci., N.Y., 1953, p. 133.

35. R. M. Noyes. J. Am. Chem. Soc., 81, 566 (1959).

36. R. M. Noyes. J. Am. Chem. Soc., 86, 4529 (1964).

37. R. M. Noyes. J. Phys. Chem., 69, 3182 (1965).

38. S. A. Levinson and R. M. Noyes. J. Am. Chem. Soc., 81, 4525 (1964).

39. J. L. Schmit. The 1984 U.S. Workshop on the Physics and Chemistry of Mercury Cadmium Telluride. May 15-17, 1984, San Diego, California. (Abstract, p. 25).

40. S. J. C. Irvine, J. Tunnicliffe, O. D. Dosser, and J. B. Mullin, ibid., p. 29.

41. D. A. Jackson. Private communication.

42. P. D. Dapkus. Ann. Rev. Mater. Sci., 12, 243 (1982).

43. S. J. C. Irvine, J. B. Mullin, and J. Tunnicliffe. J. Cryst. Growth, 68, 188 (1984).

44. S. J. C. Irvine, J. Giess, J. B. Mullin, G. W. Blackmore, and O. D. Dosser. Proc. MRS, Elsevier, N.Y., 1984. See also: Irvine, D. J. Robbins, Mullin, and J. L. Glasper, ibid.

45. A. Swollow. Radiation Chemistry of Organics, N.Y., 1961.

46. A. Charlsbie. Nuclear Radiations and Polymers, N.Y., 1961.

47. R. L. Heath. Handbook of Chem. and Phys., CRC Press, 1983-84, p. B251.

48. Isotope Products Laboratories Catalogue. Radiation Source for Research Industry. Burbank, CA, 1982.

END

5-87

DTIC